# A Case Study of Severe Storm Development along a Dryline within a Synoptically Active Environment. Part I: Dryline Motion and an Eta Model Forecast

CARL E. HANE

*NOAA/National Severe Storms Laboratory, Norman, Oklahoma*

MICHAEL E. BALDWIN

*NOAA/NWS/Storm Prediction Center, Norman, Oklahoma*

HOWARD B. BLUESTEIN

*School of Meteorology, University of Oklahoma, Norman, Oklahoma*

TODD M. CRAWFORD

*Cooperative Institute for Mesoscale Meteorological Studies, NOAA/National Severe Storms Laboratory, Norman, Oklahoma*

ROBERT M. RABIN

*NOAA/National Severe Storms Laboratory, Norman, Oklahoma*

(Manuscript received 11 July 2000, in final form 22 January 2001)

ABSTRACT

Through a case study approach the motion of a dryline (on 16 May 1991) within a synoptically active environment in the southern plains, along which severe storms ultimately developed, is examined in detail. Observations from research aircraft, surface mesonetwork stations, mobile ballooning vehicles, radar, wind profilers, and operational surface and upper air networks are examined and combined. Additionally, output from the operational mesoscale Eta Model is examined to compare predictions of dryline motion with observations and to aid in interpretation of observations.

The dryline on this day advanced rapidly eastward and included formation of a bulge; additionally, in at least two instances it exhibited redevelopment (loss of definition at one location and gain at another). Aircraft observations revealed that an eastward redevelopment occurred in the early afternoon and was characterized by a series of four ''steps'' along the western edge of the boundary layer moisture. The westernmost and easternmost steps coincide with the locations of the dryline before and after redevelopment, respectively. The retreat of the dryline in the central and southern portion of the analysis domain in the late afternoon included both continuous motion and redevelopment toward the west-northwest. This dual-mode retreat of the dryline was accompanied by gradual backing of the winds and moistening in low levels.

The Eta Model forecast initialized at 1200 UTC produced dryline features that were qualitatively similar to observed fields. The eastward motion of a broad area of enhanced moisture gradient agreed well with observations following an initial spinup period. A north–south moisture convergence axis preceded the rapid eastward motion of the dryline by several hours. Lack of subsidence in the air behind the modeled dryline leads to the conclusion that processes other than downward transfer of horizontal momentum by larger-scale motions (that would support eastward advection) produced the rapid dryline motion and observed eastward dryline bulge. Results of diagnosing physical processes affecting model dryline motion point toward boundary layer vertical mixing coupled with advection of dry air aloft as vital components in rapid advance of the dryline eastward in this synoptically active case.

## 1. Introduction

### *a. Background*

Previous observations of the dryline by synoptic-scale surface and upper air networks have shown that it can exist in both quiescent and synoptically active environments (Schaefer 1986). In the quiescent case, the motion of the dryline is dominated by vertical mixing processes related to the diurnal cycle of heating in the dry and moist air and the westward decrease in the depth of the moist boundary layer east of the Rocky Mountains. Under these conditions the dryline generally advances eastward during the daytime and retreats west-

*Corresponding author address:* Dr. Carl E. Hane, National Severe Storms Laboratory, 1313 Halley Circle, Norman, OK 73069.
E-mail: Carl.Hane@nssl.noaa.gov

ward during the evening (Schaefer 1974a,b). Within synoptically active environments, the dryline generally extends equatorward from a surface low pressure area located along a synoptic-scale frontal zone and, therefore, can be found significantly farther to the east than in the quiescent case. Motion of the dryline in this instance is modulated by the motion of the low pressure area and attendant upper-level trough's effect on horizontal and vertical air motions in addition to the vertical mixing processes mentioned above.

The dryline that is the subject of this paper developed a bulge near midday whose horizontal scale was on the order of 400 km. Eastward bulges on horizontal scales of 100–800 km sometimes occur along the dryline (Tegtmeier 1974), most frequently in the synoptically active cases. The principal cause of the bulges has been proposed to be excessive winds in the dry air, resulting in pronounced dry horizontal advection. Various processes have been proposed as the momentum source (Schaefer 1986). McGinley and Sasaki (1975), for example, have proposed that momentum is transferred by the downward branch of large-scale convective rolls, parallel to the shear, that develop as a result of baroclinic-symmetric instability.

Multiple gradients in moisture (e.g., in the case of a north–south dryline moisture gradients occurring at more than one east–west location) were also found on this day and have been documented in other cases. Tegtmeier (1974) noted cases of weaker moisture gradients or ''secondary'' drylines, along which thunderstorm activity frequently developed. These ''secondary'' drylines were located to the east of a linear area of stronger moisture gradients. Hane et al. (1993), using research aircraft and surface data, analyzed three drylines that featured multiple moisture gradients in their environment. Crawford and Bluestein (1997) used surface mesonetwork data to document multiple moisture gradients during a number of dryline passages. Hane et al. (1997), using data obtained from a sawtooth pattern flown along a dryline, found in that case that the number of moisture gradients normal to the dryline varied in the along-line direction.

The dryline that is described here moved generally eastward during most of the day, but in late afternoon and evening a segment in southern Oklahoma retreated to the west-northwest. Instances of westward retreat of drylines have been noted frequently (e.g., Fujita 1970; Bluestein et al. 1988, 1989). The physical explanation for westward dryline motion is not completely clear. Parsons et al. (1991) studied the finescale structure of a retrogressing dryline using Doppler lidar, a dual-channel radiometer, and serial rawinsonde ascents. In that case they found that hot air was riding over a westward moving denser moist flow in a manner similar to a density current. Crawford and Bluestein (1997), on the other hand, in analysis of a number of westward dryline passages using surface pressure traces, found that there were not always significant, simultaneous changes in dewpoint, wind, and pressure, as density current theory would imply.

### *b. The 16 May dryline and previous research on this case*

On 16 May 1991 a dryline was present over the experimental area. It moved eastward during the day and was associated with development of severe storms near Tulsa, Oklahoma, and south-southwest of Wichita, Kansas, near the Oklahoma border. The environment on this day was synoptically active, and the dryline moved rapidly eastward during the late morning and midday hours. It should be noted that much stronger synoptic situations than this do occur; surface winds were not sufficiently strong to produce blowing dust, and the upper-level disturbance had only modest vertical motion associated with it. In addition to surface data collected at synoptic and mesonetwork sites, profiler data, and conventional radar network and satellite data, special observations were obtained by research aircraft during all of the afternoon and by mobile sounding units during most of the day.

Previous work has also been carried out by other investigators based on data from this case. Ziegler et al. (1997) simulated this dryline convective initiation case and other cases using the Regional Atmospheric Modeling System. They employed four grids, three nested, with horizontal gridpoint separations at 60, 20, 10, and 1 km, respectively. The simulation on 16 May 1991 resulted in qualitatively accurate simulations of dryline position, cumulus development, and thunderstorm initiation in east-central Oklahoma. Bluestein and Crawford (1997) used surface mesonetwork data on this day and others to estimate terms in the equation of motion at anemometer level on either side of the dryline. In particular, 16 May data from west of the dryline were used to conclude that the vertical mixing term (of vector horizontal momentum) at anemometer level had a component normal and to the left of the surface wind. It was noted that this result is contrary to Ekman theory, possibly owing to baroclinic effects in the boundary layer.

The goal of the work that is described here is to document and better understand the detailed motion of the dryline in central Oklahoma where small-scale data were collected. This paper examines the synoptic environment, describes the motion of the dryline in detail, and uses output from the Eta Model (Black 1994) for comparison with observations, and to help understand how the synoptic scale influenced dryline motion.

## 2. Data sources and the synoptic environment

### *a. Systems utilized to acquire data*

Since large gradients in meteorological variables occur over distances much smaller than the station sepa-

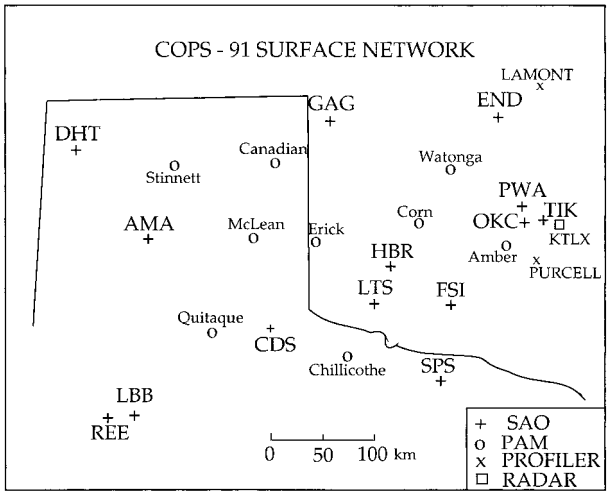


FIG. 1. Locations of surface observing sites during the COPS-91 experiments in northern Texas and western Oklahoma. PROFILER refers to sites of the Profiler Demonstration Network. Location of the KTLX WSR-88D radar is also indicated.

ration in operational networks, special observational networks are necessary to study the structure and evolution of the dryline. In recognition of this need for special observations, dryline investigations (Hane et al. 1993) were carried out during approximately seven weeks in the spring of 1991 as a part of the Cooperative Oklahoma Precipitation Studies-1991 (COPS-91). Dryline observations were collected in a region that included Oklahoma, the Texas panhandle, and southwest Kansas. Observational systems utilized during the program included a National Oceanic and Atmospheric Administration (NOAA) P-3 aircraft equipped with a large array of meteorological in situ sensors, an X-band Doppler radar, and a horizontally scanning C-band radar (Marks and Houze 1987); a pair of the National Severe Storm Laboratory mobile laboratories equipped with Cross-chain Loran Atmospheric Sounding System (CLASS) ballooning capability and continuously recording surface data systems (Rust et al. 1990); a network of National Center for Atmospheric Research (NCARs) Portable Automated Mesonetwork (PAM) stations (Brock et al. 1986); the Environmental Research Laboratories Profiler Demonstration Network (Chadwick 1988) centered in northern Oklahoma; and the Twin Lakes (National Weather Service, NWS) Weather Surveillance Radar-1988 Doppler (WSR-88D) S-band Doppler radar.

### *b. Surface and upper air analyses*

Surface observing sites in the area are shown in Fig. 1. In addition to the standard hourly observing sites, PAM sites were scattered within western Oklahoma and neighboring areas of Texas to increase resolution of surface features. Surface synoptic features are shown at 1400 UTC (0800 central standard time) on 16 May 1991 in Fig. 2a. A cold front extended from western Kansas southwestward into the Oklahoma and Texas panhandles. A dryline (marked in the figure by large horizontal gradients in dewpoint temperature) oriented north-northwest to south-southeast extended from the Oklahoma panhandle into north Texas along the west edge of a pressure trough that was centered over western Oklahoma. It is noted here that the dryline is defined by the large gradient in dewpoint or mixing ratio along the western edge of higher (and horizontally quasi-uniform) moisture to the east. Some subjectivity is necessary in the identification process owing to lack of spatial resolution in the observational set. For example, if two regions of enhanced gradient are present (i.e., one west of the other), the dryline is generally identified with the gradient that is perceived to be larger.

Surface conditions at 1700 UTC (just prior to local noon) are shown in Fig. 2b. The dryline had advanced rapidly eastward into western Oklahoma and was situated near the center of the quasi-stationary surface pressure trough. The cold front had become quasi-stationary, extending from west-central Kansas southwestward into east-central New Mexico. By 2000 UTC (Fig. 2c) the dryline extended from near Dodge City, Kansas, southeastward into central Oklahoma, then southwestward into north Texas, and was coincident with the surface pressure trough. The eastward movement of the dryline through the surface pressure trough from morning to afternoon was also noted by Crawford and Bluestein (1997). This motion through the trough is thought to be related to the diurnal heating and mixing cycle, and in this case is superimposed upon motion related to synoptic features. Apparent rapid motion across western and central Oklahoma coupled with slower movement north and south of this point resulted in the development of a pronounced meso-$\alpha$-scale dryline bulge. This is to be distinguished from bulges that can develop in the dryline on the meso-$\beta$ scale owing to local effects (e.g., see Hane et al. 1997).

Continued eastward motion of the dryline is indicated in southwest Kansas and central Oklahoma in Fig. 2d (2300 UTC). The average displacement of the dryline along its most rapidly advancing portion during the 9-h period ending at 2200 UTC was 10.7 m $s^{-1}$. This is significantly faster than the component of the surface wind normal to the dryline in the dry air. During the period of maximum eastward motion (1800–2000 UTC), the apparent average eastward speed in west-central Oklahoma was about 30 m $s^{-1}$. As will be shown later, this apparent motion actually involved redevelopment at a different location along a portion of the dryline bulge, rather than a continuous eastward movement of the dryline during this period.

At 500 hPa (Fig. 3) a closed low over southeastern Colorado moved northeastward to northwestern Kansas and filled slightly between morning and evening sounding times. An attendant trough axis extended generally south of the low into the eastern Texas Panhandle by

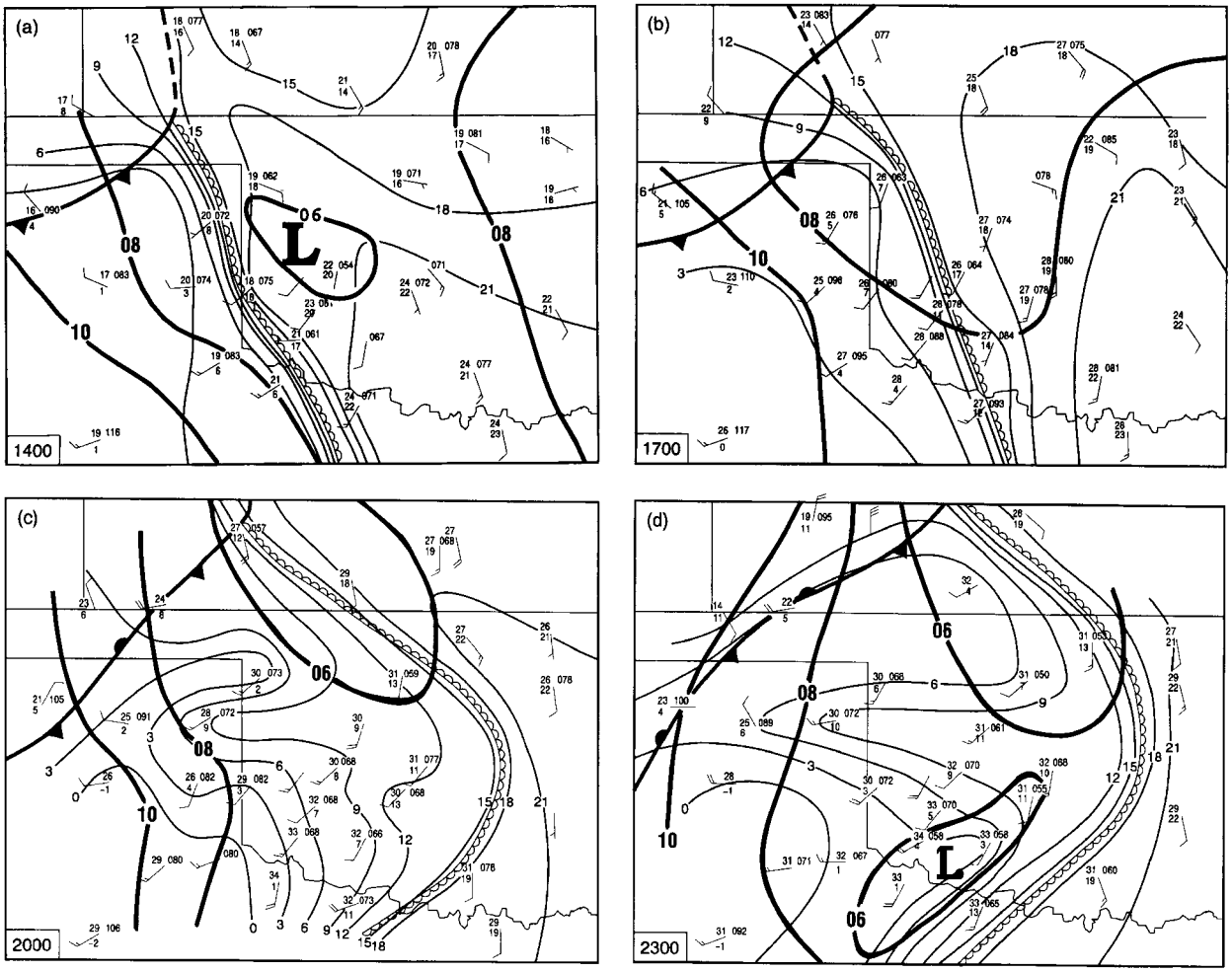


FIG. 2. Surface analysis over the area of interest on 16 May 1991 at (a) 1400, (b) 1700, (c) 2000, and (d) 2300 UTC. Dryline location is indicated by scalloped line, cold front by conventional symbol, and wind shift north of dryline–cold front intersection by dashed line. Dewpoint is analyzed at 3°C intervals (thin solid) and pressure at 2-hPa (mb) intervals (thick solid). Wind speed in station plots indicated by long and short barbs representing 5 and 2.5 m $s^{-1}$, respectively. In station model temperature (°C) is above dewpoint temperature (°C) to the left of wind indicator, and pressure (hPa tenths above 1000; e.g., 083 = 1008.3 hPa) to the right.

0000 UTC. Therefore, the dryline's relatively rapid and steady eastward motion in southern Kansas and northern Oklahoma was influenced by significant synoptic forcing (apparently through horizontal advection).

### *c. Broad view of dryline motion*

The motion of the dryline is indicated in more detail in Fig. 4, which contains an hourly isochrone analysis of dryline location between 1200 and 0000 UTC. The dryline location was determined in the 1200–1900 UTC period primarily by surface network observations, whereas after 1900 UTC (in an area where surface sites are very sparse) aircraft, radar, and satellite were the primary data sources. In particular, dryline location was denoted by a thinline within about 80 km of the Twin Lakes (KTLX) WSR-88D radar, which is located about 20 km east-southeast of Oklahoma City (see Fig. 1). Dryline motion was quite slow in the early morning. Acceleration occurred in late morning between 1500 and 1700 UTC, resulting in the rapid apparent motion over central Oklahoma noted above. In contrast the motion in the northern portion of the domain was slower and quite steady (8.5 m $s^{-1}$), but slightly faster than the northeastward motion of the upper-level low (7.5 m $s^{-1}$). The isochrone analysis reveals at least two discontinuous relocations or ''jumps'' in dryline location in central Oklahoma; an eastward relocation is apparent between 1900 and 2000 UTC, and a westward one between 2300 and 0000 UTC. As will be shown later, these relocations appear to involve a slow evolution toward a weaker moisture gradient at one location and simultaneously toward a stronger gradient at another, rather than a sudden change at both. The eastward dryline redevelopment in the 1900–2000 UTC period is superficially similar to the process of discrete frontal prop-

agation investigated by Charney and Fritsch (1999). The process that they describe involves an area of upward motion along an axis of low static stability ahead of a cold front. The upward motion is associated initially with adiabatic cooling and later with diabatic cooling (evaporation of rain) that displaces the front. The physical processes in this case are fundamentally different, aside from the weakening of a linear feature at one location and simultaneous development at another.

## 3. Analysis of aircraft and mobile sounding data relating to dryline motion

### *a. Initial aircraft soundings*

At the P-3's takeoff time (about 1700 UTC) the dryline was analyzed to be in western Oklahoma, so that aircraft observations were first focused in an area generally southwest of Oklahoma City. The P-3 first recorded a sounding from the surface to 547 hPa, centered at 1710 UTC and about 35 km west of Oklahoma City. The projection on the surface of the track (labeled 1704–1717), along which this sounding was obtained, is shown in Fig. 5 in relation to dryline location. This ascent sounding is shown in Fig. 6 and represents conditions just ahead of the eastward advancing dryline. A moist low-level layer about 60 hPa deep features well-mixed conditions and is capped by a strong inversion between 900 and 860 hPa. The depth of the moist layer and dewpoint profile in this sounding agree closely with the NWS sounding taken at Norman at 1200 UTC (not shown). Overcoming most of the cap by low-level heating would require a surface temperature of about 31°C at the base of the dry-adiabatic layer. South-southwesterly winds (Fig. 5, right) near the surface rapidly veered to southwesterly and increased in speed to 13–18 m $s^{-1}$ below 750 hPa and 23–25 m $s^{-1}$ above, in advance of the upper-level trough.

A short time later the aircraft descended to approximately 900 hPa. The location of the sounding obtained during descent is also shown in Fig. 5 (labeled 1730–1740) and is centered about 85 km west of the previous sounding and just west of the dryline. The sounding was extended linearly downward to the surface from 910 hPa using representative surface observations in the area. Dewpoints are lower at all measured levels in the latter sounding (Fig. 6), having decreased from 18° to 1°C at 910 hPa (the lowest altitude measured). Advection in addition to vertical mixing likely promoted drying in the western sounding, since moisture decreased at all levels. Based upon surface temperatures in the area of the second sounding at this time, the dry-adiabatic layer whose top is at 850 hPa extends to the surface. The inversion is clearly present in both soundings, but is approximately 50 hPa higher in the more western location. Winds from the sounding west of the dryline had a much stronger westerly component, resulting in an area of low-level convergence in the dryline zone.

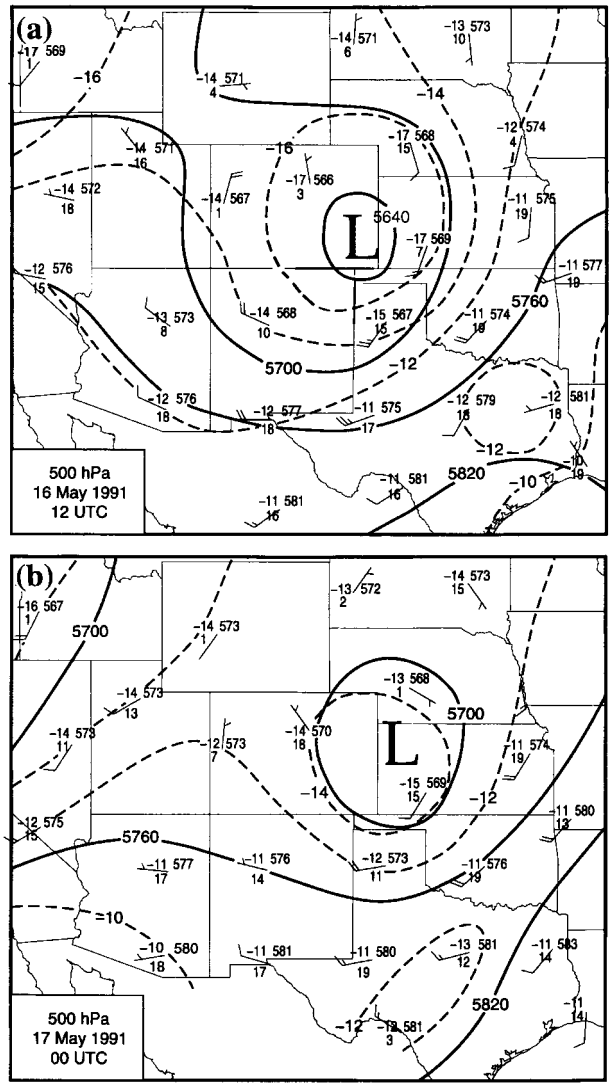


FIG. 3. Analysis of height (m, solid) and temperature (°C, dashed) fields at 500 hPa on (a) 16 May at 1200 UTC and (b) 17 May at 0000 UTC. Wind speeds are scaled as in Fig. 2. Station plots include temperature (°C, upper left), dewpoint depression (°C, lower left), and height (dm, upper right).

### *b. A vertical cross section through the dryline*

A stepped traverse pattern was flown between 1809 and 1917 UTC, centered near Binger, Oklahoma, approximately at the midpoint between locations of the two aircraft soundings. The east–west location (whose projection on the surface is shown in Fig. 5) and extent of legs within the pattern were determined on board the P-3 by keying on the moisture gradient location from the real-time aircraft measurements. Vertical cross sections resulting from this stepped traverse pattern (during which the aircraft was ascending in steps) are shown in

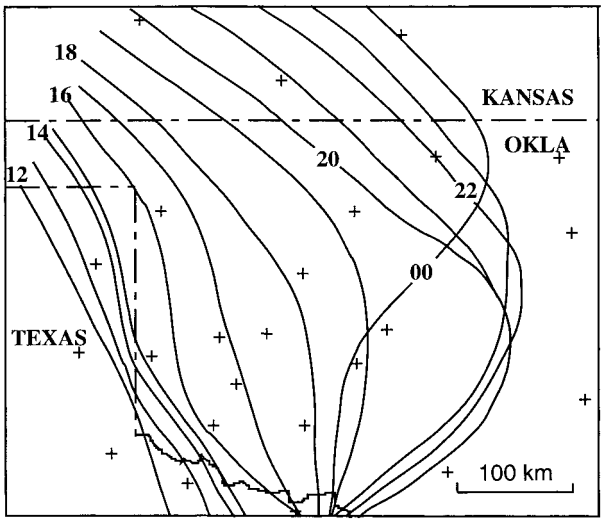


FIG. 4. Isochrones of dryline location at hourly intervals over the area of interest on 16 May 1991. Surface station locations are also indicated.

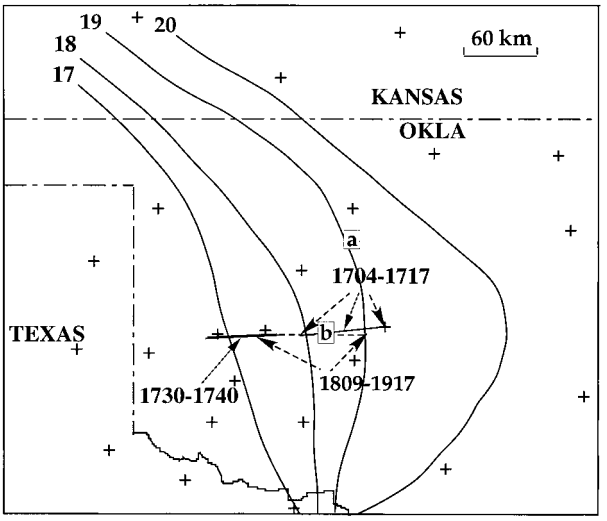


FIG. 5. Observed dryline locations at 1700–2000 UTC and locations of aircraft soundings shown in Fig. 6 and vertical cross section shown in Fig. 7. Aircraft ascent sounding is indicated by solid line (1704–1717), descent sounding by heavy solid line (1730–1740), and cross section by dashed line (1809–1917). Location of the soundings shown in Fig. 11 are denoted by a and b.

Fig. 7. It is clear from Fig. 5 that the dryline was moving rapidly eastward during the time that this stepped traverse pattern was flown. Because the dryline was moving during the pattern, a cross section plotted relative to the ground would severely distort the slope of variable fields. Therefore, the location of each observation was adjusted by taking into account estimated dryline motion (11.1 m $s^{-1}$), and the time of observation in relation to a reference time (1843 UTC, midpoint of pattern period). This procedure assumes that the variable distributions were steady during the pattern (a questionable supposition) and that dryline motion is constant with height. Thus, the analysis should be considered an approximation.

Objectively analyzed (and smoothed) water vapor mixing ratio is shown in Fig. 7a over an east–west distance of 80 km and a depth of 900 m. The dryline location is evident between +12 and +22 km; however, its structure is not as well defined as in other cases similarly depicted in the past (e.g., see Ziegler and Hane 1993; Hane et al. 1993, 1997). The adjustment for dryline motion results in an apparent westward displacement of legs as altitude increases. The strong moisture gradient in the easternmost 2 km of the fourth leg (counting from bottom to top) is likely the western edge of upwelled moisture associated with the dryline circulation. However, the narrow maximum (in excess of 7.5 g $kg^{-1}$) extending above 1.3 km at $x = 14$ km is a separate feature (assuming that the dryline motion was uniform with height). Based upon the sounding shown in Fig. 6, the depth of the moist layer east of the dryline was about 600–700 m, so that the flight leg at about 1.35 km was likely just above this moist layer. The vertical orientation of isolines west of $x = 20$ km and below $z = 1.1$ km is indicative of vigorous vertical mixing in the dry air. The decrease in mixing ratio eastward from $x = 27$ km may be an indication that downward motion (the downward branch of the dryline circulation) was effectively isolating this area from abundant moisture to the east. Kinematically derived vertical motion (not shown) in the cross section shows alternating columns (2–3 km wide) of upward and downward motion in this area.

In Fig. 7b an objective analysis (also adjusted for line motion and spatially smoothed) of the u-component (east–west) wind is shown. There is a minimum of westerly component in the lower-right portion of the cross section, and weak *u*-component convergence in low levels (implying upward air motion) near $x = 27$ km coincides with the eastern edge of the moisture gradient shown in Fig. 7a. Most of the remainder of the cross section is characterized by weak vertical shear and small

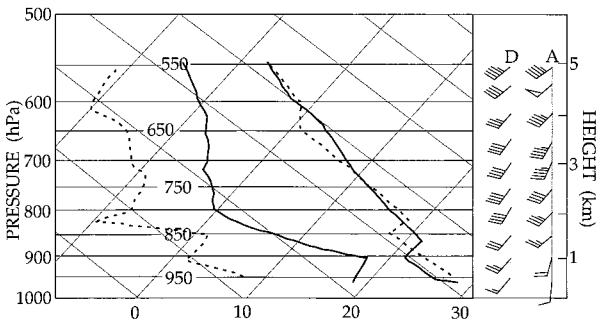


FIG. 6. Aircraft ascent sounding (solid) and descent sounding (dashed) centered at 1710 and 1735 UTC, respectively, from locations noted in Fig. 5. Inset shows aircraft wind profiles from descent (D) and ascent (A) soundings with wind speed noted as in Fig. 2 (with addition that flag denotes 25 m $s^{-1}$ wind).

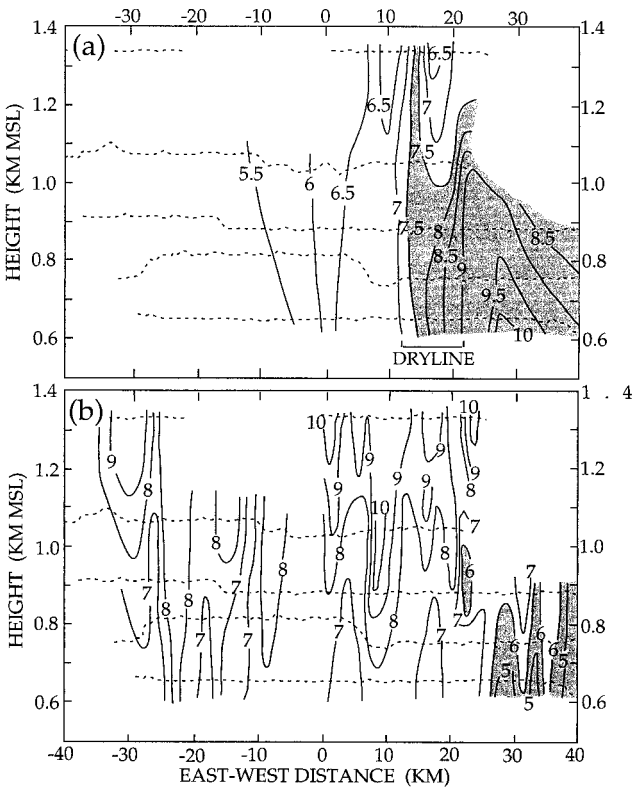


FIG. 7. East–west cross section showing (a) water vapor mixing ratio (g kg$^{-1}$) and (b) $u$ component of air motion (m s$^{-1}$) derived from the 2150–2328 UTC aircraft stepped traverse pattern whose location is shown in Fig. 5. Dotted lines indicate projection of aircraft track in this cross section. Mixing ratios in excess of 7.5 g kg$^{-1}$ and wind components less than 6 m s$^{-1}$ are shaded.

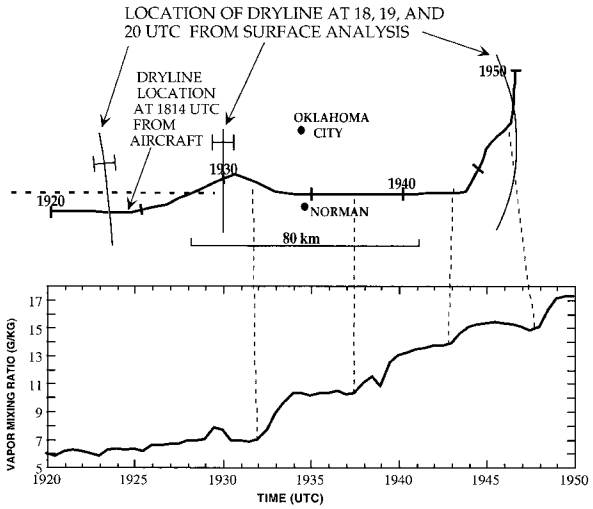


FIG. 8. (top) Track of aircraft through central Oklahoma with time (UTC) noted, dryline isochrones (light, solid, with estimated error bars) at various times, and location of vertical cross section (heavy dashed) shown in Fig. 7. (bottom) Time series of water vapor mixing ratio (g kg$^{-1}$) along the track.

oscillations in velocity on a horizontal scale less than 10 km. One exception to this structure is the maximum in $u$ component ($>$10 m s$^{-1}$) near $x = 10$ km that is located just west of the strong moisture gradient associated with the dryline.

### c. *Multiple moisture gradients and dryline redevelopment*

#### 1) OBSERVATION OF MOISTURE GRADIENTS

Following completion of this stepped traverse pattern, the aircraft descended to low levels (approximately 925 hPa) and headed east. In Fig. 8 the track of the aircraft between 1920 and 1950 UTC is plotted along with the corresponding time series of water vapor mixing ratio from the aircraft sensor. The heavy dashed line marks the location of the earlier stepped traverse pattern. The moisture data were filtered by averaging over 40 s at 30-s intervals. By the end of this time period the dryline was located at the rather sharp increase in moisture that occurred between 1948 and 1949 UTC. The mixing ratio change along the aircraft track between 1932 and 1949 UTC was from 7 g kg$^{-1}$ to more than 17 g kg$^{-1}$, respectively, over an east–west distance of approximately 90 km. This increase occurred predominantly in a series of four steps, each of whose beginning point is marked in Fig. 8 in the time series and along the track. Each step consisted of a strong gradient of approximately 7–15-km width followed by a nearly constant or slowly increasing region. The east–west distance between these increases was approximately 35, 31, and 20 km (beginning with the westernmost interval).

The dryline location at various times is indicated in the top portion of Fig. 8. The speed indicated between 1800 and 1900 UTC is about 11 m s$^{-1}$ toward the east. For verification the aircraft measurement of dryline location is noted at 1814 UTC, and the agreement is reasonable, given the uncertainty of the position based on surface network data. If it is assumed that the moisture gradient centered on 1933 UTC in the time series is the same feature that had earlier been identified as the dryline, and its motion calculated, the resulting speed is about 11.7 m s$^{-1}$. If the aircraft measurements at 1814 and 1933 UTC are used alone, the speed calculated is 10.7 m s$^{-1}$. It is therefore most probable that the 1933 UTC gradient measured by the aircraft is the feature that was earlier identified as the dryline.

It is concluded that the nature of this discontinuous change in location is likely the result of a gradual weakening of the dryline signature in the western location and a strengthening in the eastern location. Evidence of this is shown in Fig. 9 where time series of dewpoint temperature are plotted at three PAM sites. At the Corn and Watonga sites (see Fig. 1) the decrease in moisture is more rapid and larger than at the more eastern location (Amber). At Amber the total decrease in moisture takes place more gradually, more consistent perhaps with a

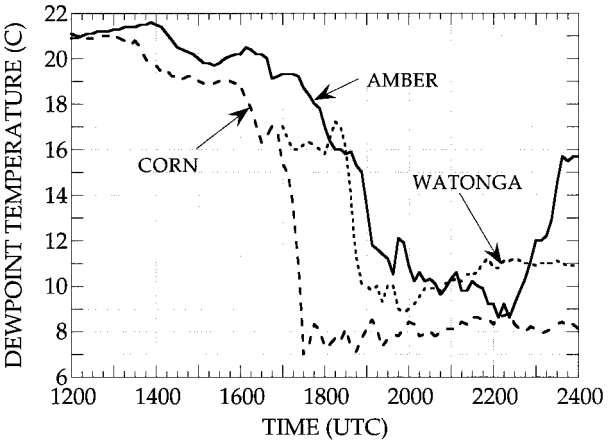


FIG. 9. Dewpoint temperature (°C) as a function of time (UTC) at the Corn, Amber, and Watonga PAM sites.

weakening of the dryline at the western location, strengthening to the east, and passage of the western moisture gradient.

In Fig. 10 reflectivity from the KTLX WSR-88D is shown near the time of the time series of Fig. 8. The dryline location is the distinct thinline in the eastern half of the figure. The more prominent thinlines west of the dryline are highlighted, and the time at which each thinline was crossed by the aircraft is noted. Comparison of thinline locations with moisture steps shown in the Fig. 8 time series reveals a fairly good correspondence between thinlines and steps, though the 1938 thinline is lost in ground clutter and the 1943 thinline is not distinct at the crossing point. Therefore it appears that the moisture steps shown in Fig. 8 are likely continuous features along the thinlines over distances of at least 100 km.

### 2) DISCUSSION

A number of questions arise based on these observations. How did the evolving gradients in moisture and any accompanying convergent signatures arise in the deeper moisture east of the dryline prior to the 1930–1950 measurements? Had this process been going on for many hours or did it occur rapidly? Did the formation of all the ''steps'' along the western edge of the moist layer occur simultaneously or in sequence? Did the larger scale have an influence on the process? Does this sort of thing occur often with synoptically influenced drylines, and does it occur also with ''quiescent'' drylines? Unfortunately, the temporal and spatial scale and intermittency of this dataset do not allow these questions to be answered. It is known that multiple gradients are present in the dryline environment from observations (see, e.g., Hane et al. 1993; Crawford and Bluestein 1997; Hane et al. 1997), and from one model simulation (Shaw et al. 1997). Eastward redevelopment in a quiescent dryline case was noted by Hane et al. (1997).

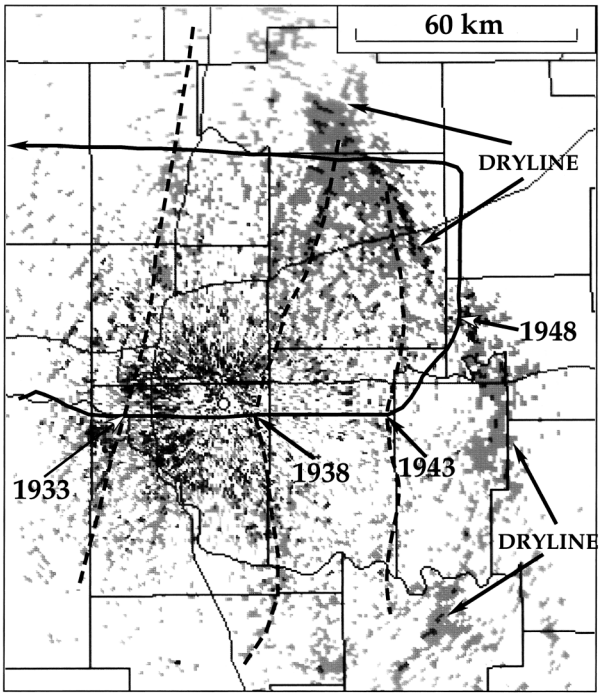


FIG. 10. Reflectivity from the KTLX WSR-88D at 1935 UTC. Reflectivity shadings (gray, black) are centered at 5 and 10 dB*Z*, respectively. Dashed lines highlight thinlines mentioned in text. Solid line is aircraft track with thinline crossing times noted.

In that case the displacement was likely strongly influenced by the character of the soil composition and vegetative cover at the surface and heating rates above it. With the knowledge that redevelopments take place in some cases, it is easier to understand why surface data analysts in both operational and research settings find placement of the dryline challenging. In some cases attempting to incorporate a continuous dryline motion from one analysis time to the next is simply not appropriate.

It has been speculated previously (Hane et al. 1993; Ziegler and Hane 1993; Ziegler et al. 1995; Shaw et al. 1997) that compensating downdrafts east of the dryline may be involved in producing multiple gradients. There is some evidence, for example in the vertical velocity measurements made directly by the aircraft (not shown), that differential vertical motion in the east–west direction occurs on the same spatial scale as the steps in the moisture field. If this is the case, then it would seem that there is some wave structure in place. Such waves might develop simultaneously or perhaps sequentially, with successive steps developing farther to the east with time. This then raises the question as to why a particular step evolves into the newly relocated dryline.

A field of horizontal convective rolls (HCRs) is one type of structure that might be consistent with the observations within the region of redevelopment. Atkins et al. (1998) showed clear examples of HCRs in the environment of a dryline on the basis of WSR-88D and

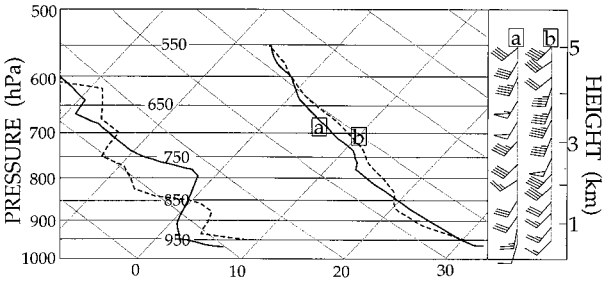


FIG. 11. Mobile-CLASS soundings taken on 16 May 1991 at (a) 2103 (solid) and (b) 1917 UTC (dashed). Locations are indicated in Fig. 5. Inset on right shows wind profiles, with wind speed noted as in Fig. 5.

aircraft data. The linear structures oriented toward the northeast, located just west of the westernmost marked thinline in Fig. 10, are likely HCRs, owing to their regularity and relatively small wavelength. The question, however, concerns the two thinlines with crossing times marked 1938 and 1943 in the figure. In order for HCRs to be present in this region the environmental conditions must be supportive of their existence.

Over the last few decades field studies have been designed to better understand preferred environments for rolls and various roll characteristics (e.g., LeMone 1973; Grossman 1982; Weckwerth et al. 1997). Some studies have indicated that thermal instability and a mean convective boundary layer (CBL) wind speed of at least 5 m $s^{-1}$ are necessary for convective roll development. Most observational, modeling, or theoretical studies have indicated the mean CBL wind shear should fall in the $10^{-3}$ to $10^{-2}$ $s^{-1}$ range. Other observational studies have demonstrated that rolls can develop at much lesser wind speeds, provided that sufficient sensible surface heat flux is present (Weckwerth et al. 1999).

A sounding taken at 2103 UTC about 20 km south of Enid, Oklahoma (location noted in Fig. 5), and about 80 km west of the dryline is shown in Fig. 11. A second sounding is also shown in Fig. 11 and was taken at 1917 UTC about 50 km west of Oklahoma City and 40 km or more west of the dryline. The CBL depth (depth of the quasi-dry-adiabatic layer near the surface) ranged from about 900 m (Figure 11, curve b) to 1900 m (curve a) in these soundings and the mean boundary layer wind was about 13 m $s^{-1}$ from 220°. If the two thinlines depicted in the Fig. 10 radar image immediately to the west of the dryline are identified as horizontal convective rolls, a mean roll orientation toward the north-northeast is indicated. It should be noted that WSR-88D radars are limited in their detection of horizontal convective rolls both by their relatively long wavelength, by strong range dependence, by their inability to detect weaker roll circulations, and by the fact that structures other than HCRs can produce thinlines. However, assuming that these thinlines are HCRs, both the along-roll and cross-roll mean CBL shear, from the above-mentioned soundings, are approximately $5 \times 10^{-3}$ $s^{-1}$. There is general agreement that roll wavelength is dependent upon CBL depth, and in most cases the ratio of roll wavelength to CBL depth (aspect ratio) has been observed to be approximately in the 2–7 range. In this case the aspect ratio (if rolls are being observed) is in the 9–36 range, higher than measured in most field studies. Larger aspect ratios have been attributed by past investigators to high wind speeds in a neutral or unstable environment or larger mean CBL vertical wind shear. It appears that the observed environment was one in which rolls might have formed, but observations on finer temporal and spatial scales would have been necessary to confidently identify the two thinlines west of the dryline in Fig. 10 as HCRs.

### *d. Cause of redevelopment along a limited sector of the dryline bulge*

A brief recounting of the nature of dryline eastward motion in Oklahoma and southern Kansas includes, first, the development of an east-northeastward bulge in the 1700–1900 UTC period. This bulge can be seen, for example, in Fig. 5. Between 1900 and 2000 UTC an eastward redevelopment of the dryline took place resulting in the large displacement along a portion of the dryline bulge area in central Oklahoma. An important remaining question is how conditions in this area contributed to the redevelopment along this sector of the dryline, but not in areas farther to the north, for example. To address this question properly would require a comparison of small-scale observations along the redevelopment sector *and* in the area farther north. The above analyses, based on aircraft data for the most part, have shed some light on structures within the redevelopment region. Unfortunately, detailed observations are not available farther to the north, owing to the limited area that a single aircraft can sample during a given period. In a later section of this paper a model simulation of this case is described. It will be seen that the model does predict a modest bulge in Oklahoma, but no redevelopment along a portion of the bulge. Therefore the model output does not contribute to understanding the cause of redevelopment.

The scant information available pertaining to this question is in the form of soundings and wind profiles. The soundings that are most pertinent here are shown in Fig. 11. The sounding labeled (a) was taken very near the northern edge of the redevelopment area, while sounding (b) was within the redevelopment area. Time series of wind profiles (hourly, not shown) were examined from profiler sites at Lamont, Oklahoma, in the area north of where redevelopment took place and at Purcell, Oklahoma, within the region of redevelopment. The outstanding feature of the soundings in Fig. 11 is the fact that the depth through which boundary layer mixing took place to promote advancement of the dryline was significantly greater at the northern site than that within the redevelopment region. Quasi-adiabatic

conditions extending up from the surface are present in the northern location through a depth of about 2.1 km, whereas a similar layer was only about 0.9 km deep within the redevelopment region. The wind shift at dryline passage from the profiler data occurred through a depth of approximately 2.5 km at the Lamont site (northern) and through less than 1 km at Purcell. Thus, evidence from independent sources points toward dryline advancement by mixing through a relatively shallow depth within the along-dryline segment where redevelopment occurred. To better understand why this differential mixing depth was present and how it influenced redevelopment would require more sounding information at along-line points ahead of the dryline, additional aircraft data in locations where redevelopment did not occur, and clear air radar data from additional sites.

## 4. Structure and motion of the dryline in east-central Oklahoma in late afternoon

To complete description and analysis of dryline motion on this day, attention is now focused on a retreating segment of the dryline in the late afternoon. The portion of the dryline south of the bulge both retreated continuously in the 2100–0000 UTC period and redeveloped westward between 2300 and 0000 UTC. Storm initiation on retreating drylines has been documented on many occasions (e.g., Fujita 1970; Bluestein et al. 1988, 1989), and therefore the motion of this boundary is an important consideration in nowcasting storm initiation. The dryline's westward redevelopment, based upon hourly surface observations, is illustrated in Fig. 12. In the northern portion of the domain it continued its advance toward the northeast, whereas in the southern portion a westward redevelopment is evident, based on backing of the winds and pronounced increase in moisture at the Oklahoma City and Amber surface sites.

In Fig. 13 isochrones of dryline and thinline locations based upon KTLX clear air data are plotted on the reflectivity image at 2230 UTC. Isochrones of the thinline southeast of the radar representing the dryline are plotted from 2108 to 0002 UTC. As noted previously, the dryline redeveloped farther west (at location of the distinct westernmost thinline in Fig. 13) so that the later isochrones southeast of the radar (e.g., that at 0002 UTC) represent a thinline that remained after the westward redevelopment. The thinline whose motion is represented by the set of isochrones from 2200 to 0031 UTC in the western part of the domain was quasi-stationary until about 2230 UTC then also began to retreat toward the northwest at an average speed of 6 m $s^{-1}$. This is comparable to the speed of retreating drylines investigated in the past [8–9 m $s^{-1}$ in the cases studied by Fujita (1970), Bluestein et al. (1988), and Bluestein et al. (1989)], but considerably faster than the dryline/thinline westward speed southeast of the radar on this day (3.6 m $s^{-1}$).

The inset in Fig. 13 shows the time history of dew-

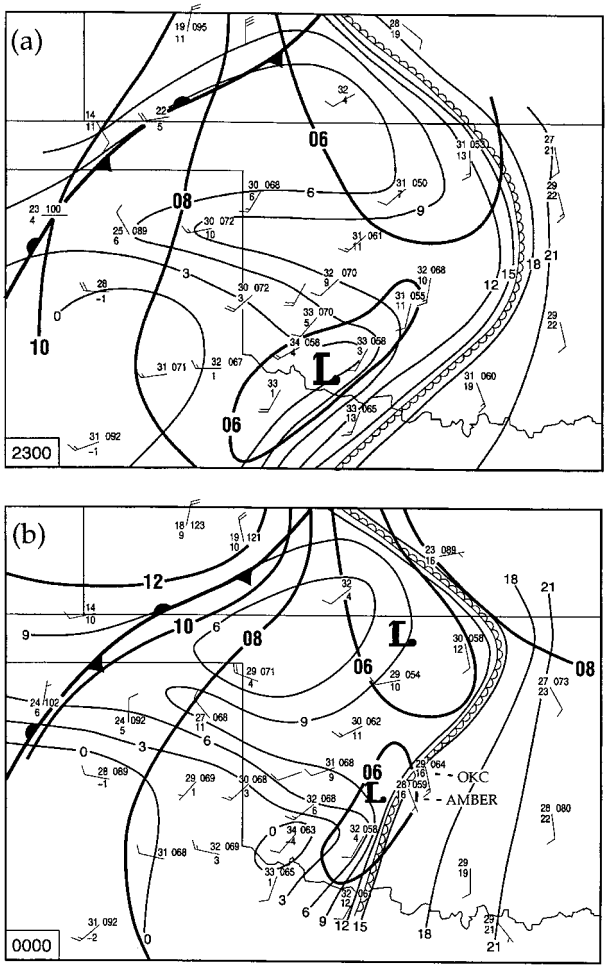


FIG. 12. Surface analyses as in Fig. 2 but at (a) 2300 UTC on 16 May 1991 and (b) 0000 UTC on 17 May 1991, where locations of the Oklahoma City (OKC) and Amber surface sites are indicated.

point temperature and wind direction between 2200 and 0000 UTC at the Amber PAM site, whose location is also noted in the figure. The thinline/redeveloping dryline passed northwestward over the site beginning at about 2322 UTC based both on the measurements at the surface site and the clear air radar return. An abrupt increase in dewpoint and backing of the wind occurred simultaneously. There was also a slower moistening and backing of wind at the site in the hour preceding passage of the boundary, indicating that these changes were taking place in the larger-scale environment on both sides of the boundary. In Fig. 12 at both 2300 and 0000 UTC low pressure is indicated in southwest Oklahoma. At the earlier time the dryline is clearly to the east of the low pressure area, whereas an hour later the dryline is nearly coincident with the low. Thus, the larger-scale backing of the wind and advection of moisture to the west may have been in part a response to lowered pressure to the west that was present during much of the afternoon.

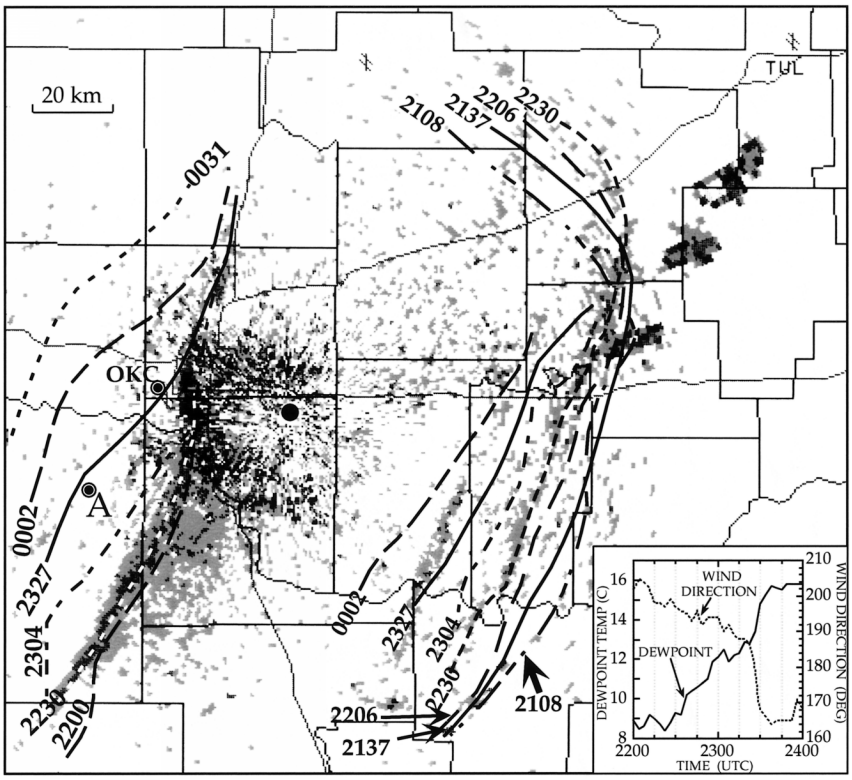


FIG. 13. Isochrones of thinline motion at labeled times superimposed upon reflectivity (dB*Z*) from the KTLX radar at 2230 UTC on 16 May 1991. Reflectivity levels in clear air return are centered on 5 and 10 dB*Z*, while maximum reflectivity in the northernmost precipitating cell is about 40 dB*Z*. Inset at lower right shows time series of dewpoint temperature and wind direction at the Amber, OK, site, whose location is noted by A.

In addition to the two prominent thinlines highlighted in Fig. 13, there are other less distinct, but persistent, thinlines present in the clear air return. One of these is oriented generally parallel to the dryline south of the bulge and appears to intersect the dryline north of the bulge. It is spaced 15–20 km west of the dryline (or easternmost thinline) and is best seen in Fig. 13 south of the figure's midpoint. This secondary line also retreated to the west-northwest (not shown), maintaining nearly constant distance from the dryline. A third less distinct thinline is present at times, spaced 15–20 km west of the secondary line, and also intersects the dryline north of the bulge. This third thinline is best seen in Fig. 14, which contains KTLX reflectivity from clear air targets and from three thunderstorm cells east of the dryline at 2241 UTC. The events surrounding the initiation of these storms will be described in a future publication. The dryline location is noted, as are the secondary and tertiary thinlines west of the dryline. The research aircraft executed a stepped traverse pattern across the dryline between 2150 and 2328 UTC from which a vertical cross section was produced in the location marked in Fig. 14. The cross section also included a crossing of the tertiary thinline.

The vertical cross section through the dryline and tertiary thinline is shown in Fig. 15. Data in the cross section verifies that the prominent easternmost thinline in the radar images is produced by the dryline, and also illustrates the two-dimensional structure just to the north of the area where retrogression took place. The dryline was moving slowly eastward during approximately the first half of the period of data collection for this cross section and was stationary thereafter. In a trial analysis, correction was made for this motion in constructing the cross section; however, there was little change in the overall analysis aside from a slightly more vertical slope in some features (e.g., the strong gradient along the west edge of the moist pool). Therefore, the uncorrected analysis is shown in Fig. 15. It is also noted that the aircraft crossed the dryline and tertiary line along its lowest leg at approximately 2210 UTC, so that the cross section extended farther east of the dryline than indicated in Fig. 14. The distance between the dryline and tertiary line in the cross section (Fig. 15a) is about 13 km; this agrees very closely with the radar image at 2212 UTC (not shown).

Convergent signatures in the lowest levels found in the east–west wind component (Fig. 15b) coincide with the dryline and tertiary line moisture gradients. The convergence associated with the tertiary line is much

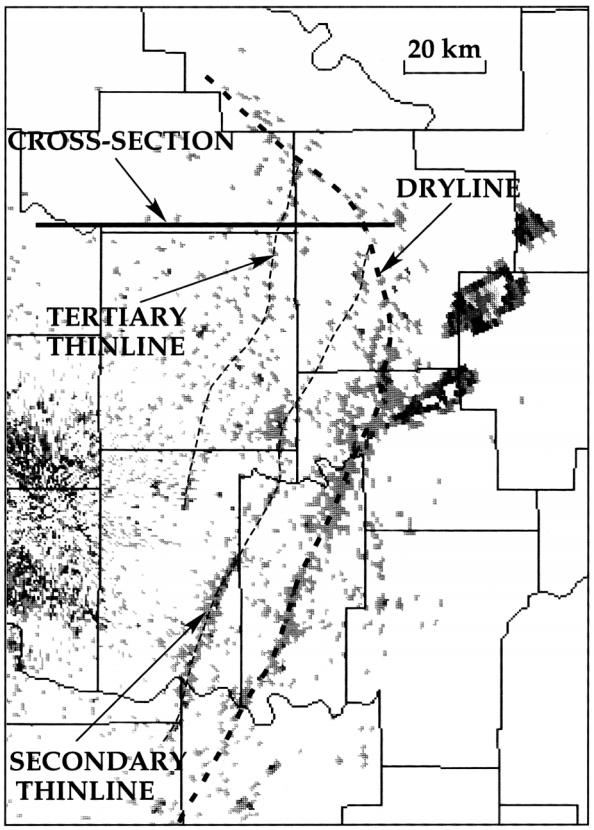


FIG. 14. Reflectivity at 2241 UTC on 16 May 1991 with location of Fig. 15 vertical cross section indicated. Maximum reflectivity in thunderstorm cell is in excess of 50 dBZ. Bold dashed line marks dryline location and thin dashed lines other thinlines.

shallower than that with the dryline. As in other dryline cases, there is large vertical shear in both the east–west component and north–south component (not shown) east of the dryline compared to that to the west. This is consistent with the high degree of vertical mixing that takes place to the west of the dryline. A vertical motion field, highlighted in Fig. 15c and derived from the objectively analyzed east–west component of motion and upward integration of the anelastic continuity equation, includes a number of small-scale areas of upward motion located at and to the east of the tertiary thinline. Strongest upward motion is near the dryline, and in the 0.5–1.0 m $s^{-1}$ range. Cross sections through other drylines (e.g., on 15 and 26 May 1991), based on data from the same type pattern and using the same analysis technique, have yielded vertical motions that are on the order of twice this magnitude. In these other cases the low-level easterly wind component east of the dryline appeared to be deeper and low-level convergence and moisture gradient restricted to a smaller horizontal distance. Changes in moisture and wind component in this case occur over a greater horizontal distance, with most pronounced changes occurring at the dryline and tertiary thinline.

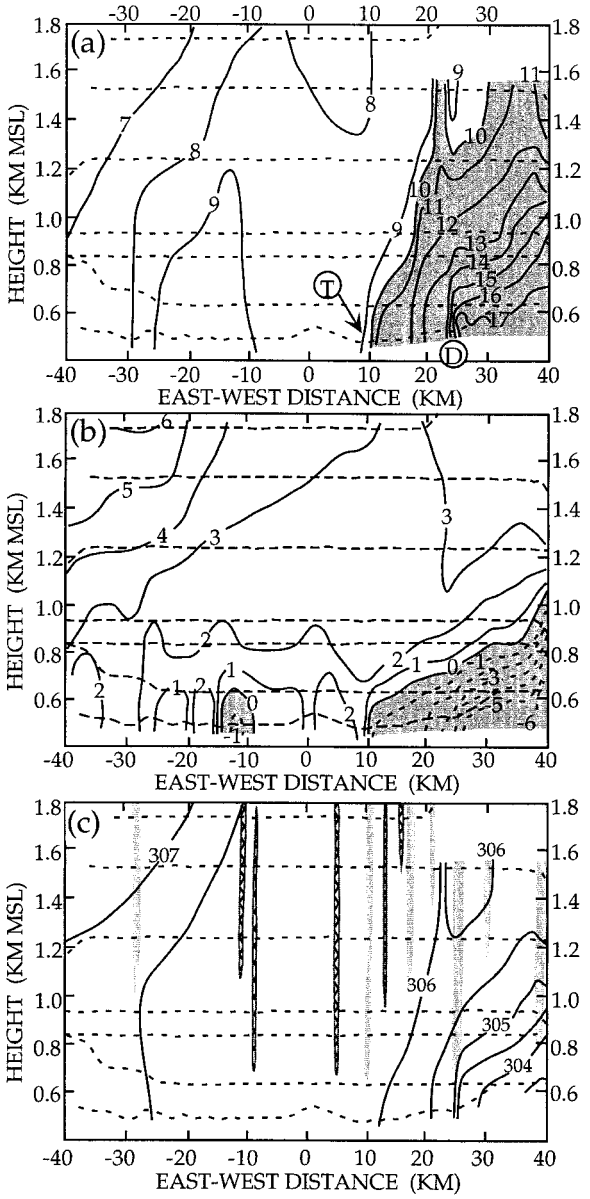


FIG. 15. Vertical cross section through the dryline at the location shown in Fig. 14, based on aircraft data collected from 2150 to 2328 UTC. Dashed lines indicate track of aircraft. Contoured fields are (a) water vapor mixing ratio (g $kg^{-1}$), where circled D and T mark locations of dryline and tertiary thinline, respectively; (b) east–west wind component (m $s^{-1}$); and (c) potential temperature (K) with superimposed maxima of upward and downward motion. Upward motion is gray (>0.5 m $s^{-1}$) and downward is hatched (<0.5 m $s^{-1}$).

From Fig. 14 it is clear that the dryline–thinline structure is not two-dimensional at this particular location, since the thinline is not parallel to the dryline. Therefore the structure depicted in Fig. 15 is expected to vary with along-line location along *this section* of the line. However, farther south (as little as 40 km) the secondary thinline is quasi-parallel to the dryline so that it is possible that the structure is more two-dimensional and

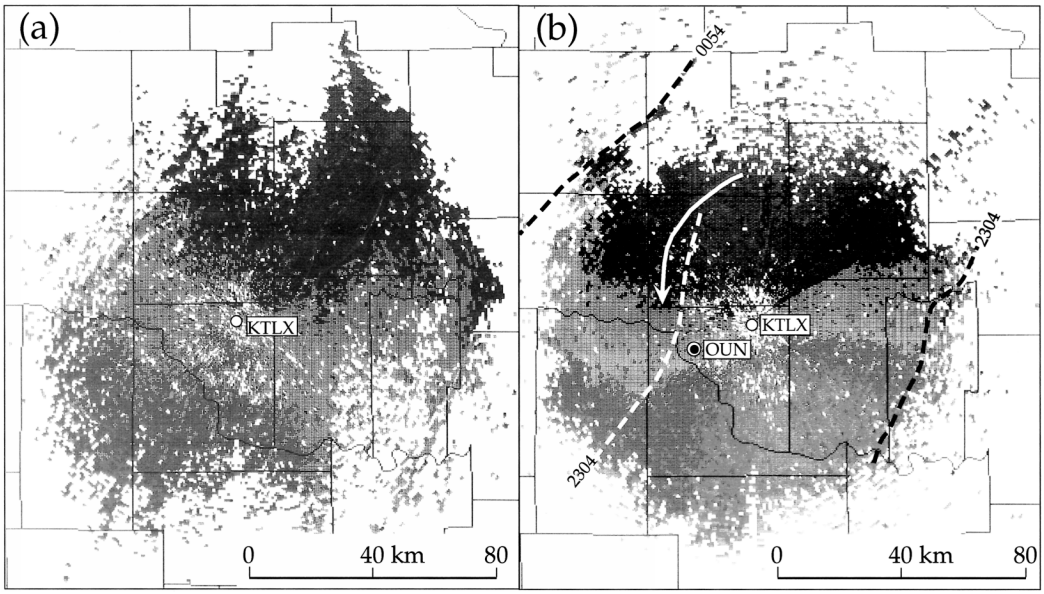


FIG. 16. Radial velocity field from the KTLX radar at (a) 2027 UTC on 16 May and (b) 0054 UTC on 17 May. Lighter shading generally east and west of the radar represents radial velocities in the $-2.5$ to $+2.5$ m s$^{-1}$ range. Darker shading north of the radar represents radial velocities greater than $+2.5$ m s$^{-1}$ (away from the radar) and intermediate shading south of the radar denotes radial velocities less than $-2.5$ m s$^{-1}$ (toward the radar). In (b) dashed lines mark locations of thinlines, the curved arrow denotes the location of 0055 UTC aircraft sounding, and OUN the location of the 2307 UTC Norman sounding.

similar to that depicted in Fig. 15. Unfortunately no cross section is available along that portion (south of the bulge) of the dryline.

As noted above, there appeared to be larger-scale backing of the wind and moistening in the area where the dryline retreated. Additional observations show that these changes took place not only at the surface, but through much of the boundary layer. Figure 16 shows the radial velocity field from 0.5° KTLX elevation scans at two times. In Fig. 16a the pattern at 2027 UTC (mid-afternoon) is shown. Low-level winds are from about 210° at 5 m s$^{-1}$, while winds at a height of approximately 1 km are from the same direction at about 15 m s$^{-1}$. This is consistent with well-mixed conditions west of the dryline. By 4 h later the wind profile had changed significantly, as indicated by the radial velocity field at 0054 UTC shown in Fig. 16b. Near-surface winds are from about 170° at about 7 m s$^{-1}$, while winds at approximately $z = 1$ km are from about 180° at about 17 m s$^{-1}$. This wind structure is characteristic of a location east of the dryline. Inspection of the radial velocity fields at intervening times confirms that the change took place gradually at the radar site, consistent with a larger-scale influence rather than with the passage of a wind shift line over the site. A part of this backing may have resulted from processes in the diurnal cycle, wherein in late evening a loss of vertical mixing owing to reduced solar heating decouples near-surface momentum from that at higher levels (Bluestein and Crawford 1997). Radial velocity measurements do not extend high enough to confirm or refute this.

Additional data on changing conditions in the boundary layer and slightly higher are provided by soundings in this area. The Norman National Weather Service 0000 UTC sounding was released at 2302 UTC from the location noted in Fig. 16b (OUN). A representative time for measurements in the lower 300 hPa of the atmosphere is about 2307 UTC. A second sounding was derived from data collected by the research aircraft during its landing approach toward Will Rogers Airport. The aircraft track between the 800-hPa level and the surface is noted in Fig. 16b, was centered about 40 km north of the OUN sounding, and was assigned a representative time of 0055 UTC. Figure 16b also shows the location of the thinlines associated with the dryline (black dash at 2304 and 0054 UTC) and convergence line (white dash) near the sounding times. The OUN sounding was taken just east of the thinline (marked 2304 in Fig. 16b) that would later become the relocated dryline. The aircraft sounding was taken about 1.8 h later, and by this time the dryline had retreated northwestward (to the 0054 location noted in Fig. 16b). Therefore, this sounding was positioned 35–45 km southeast of the dryline. The thinline to the east that had earlier marked the dryline was by this time not present in the radar return.

The two soundings are shown in Fig. 17. Significant changes occurred between the two sounding times in temperature, moisture, and wind structure. Winds backed near the surface and strengthened between the surface and 820 hPa, as indicated in Fig. 17b. Below 900 hPa there was an increase in moisture with little change in temperature (Fig. 17a). Between approxi-

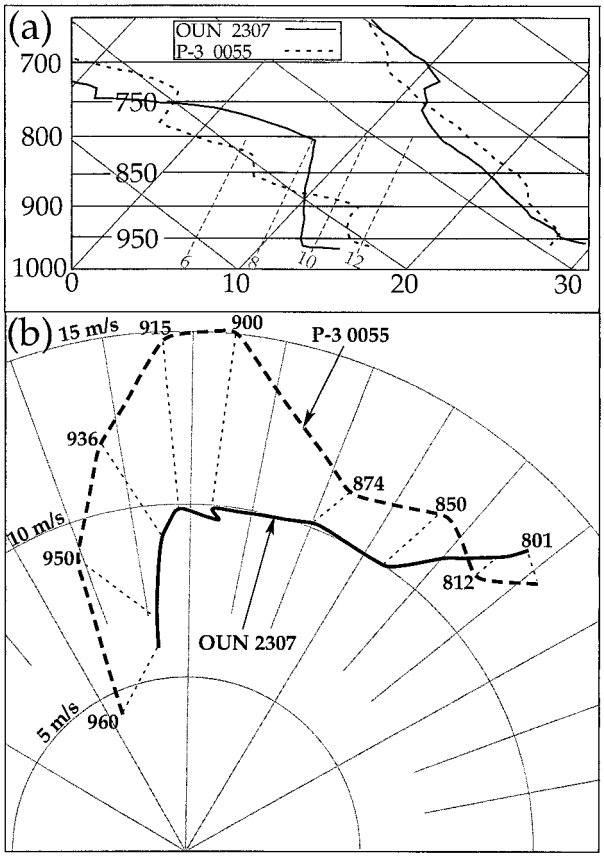


FIG. 17. Soundings from OUN at 2307 UTC on 16 May and from aircraft at 0055 UTC on 17 May at locations noted in Fig. 16. Shown are (a) skew *T* diagram for OUN (solid) and aircraft (dashed) from surface to 650 hPa, and (b) hodograph from surface to 800 hPa. Pressure (hPa) along P-3 (aircraft) curve is noted, and lightly dashed lines point to corresponding pressure along OUN hodograph.

mately 900 and 750 hPa, there was warming and drying. The depth of the near-surface moisture increase coincides well with the depth of the strong south-southeasterly to southerly winds in the later sounding. Therefore the reason for this moistening is likely horizontal advection. The wind veers rapidly above 900 hPa, coincident with a thermal stable layer and rapid drying in the later sounding. The drying and warming above 900 hPa results from either horizontal advection of warm dry air from the southwest or subsidence. The changes exhibited between these two soundings are consistent with dryline retreat to the northwest, where the second sounding is much farther east of the dryline; however, the depth of the low-level moist layer at this time is shallow compared to the depth in the afternoon before dryline passage.

In the next section results of an Eta Model (Black 1994) simulation will be used to gain understanding of how larger-scale processes may have contributed to the dryline motion and evolution on this day. In the absence of subsynoptic-scale observations with time and space resolution sufficient to explore larger-scale influences, a mesoscale model producing a reasonably accurate simulation is a potentially valuable research tool.

## 5. Eta Model simulation

### *a. Model description*

In order to explore the possible influence of the larger scale on the dryline motion, structure, and evolution, and more generally, to assess the ability of an operational model to predict the presence, location, and movement of the dryline on this day, a mesoscale model was utilized. The Eta Model (Black 1994), an operational mesoscale model running at the National Centers for Environmental Prediction (NCEP), was run after the fact using archived data for initialization. Versions of this model with approximately 30-km horizontal grid spacing have been used operationally to provide guidance in mesoscale forecasts since mid-1994.

The configuration of the mesoscale Eta Model that was employed in this investigation was nearly identical to the operational version that was running at NCEP in July 1998 (Rogers et al. 1997). The model structure included a grid network with 32-km grid spacing in the horizontal and 45 layers in the vertical over a domain of approximately 6000 km by 4700 km covering most of North America. The physical processes used in the model included an explicit cloud prediction scheme (Zhao et al. 1997), a sophisticated land surface model (Chen et al. 1996; Betts et al. 1997) including four layers of prognostic soil temperature and moisture, and a revised version of the Mellor–Yamada level 2.5 turbulence scheme (Janjić 1996b). Initial and boundary conditions for this case were obtained by direct interpolation of archived fields from the NCEP–NCAR reanalysis project (Kalnay et al. 1996). It should be noted that analyses were used for boundary conditions rather than a global model forecast. This mode of boundary condition specification could not be employed in an operational environment. However, the impact of the boundary conditions was likely insignificant since only the first 12 h of a 36-h forecast were examined over the center of the computational domain. Output was obtained via the same postprocessing routines as were used operationally, with fields interpolated from the model grid to a 40-km Lambert conformal grid with 25-hPa vertical spacing.

### *b. Limited comparison of model results with observations*

In attempting to use model output to explore larger-scale influences on the dryline on this day, it was necessary to determine the accuracy of the simulation. The model, whose horizontal grid spacing is 32 km, cannot resolve the finescale structure of the dryline. It can, however, resolve moisture and wind features on a larger

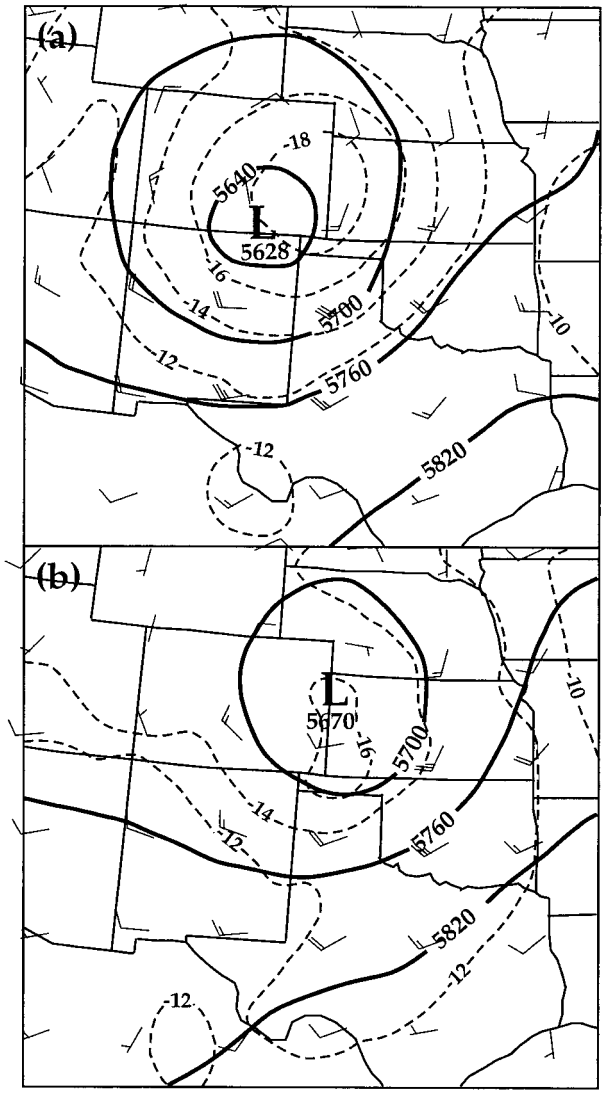


FIG. 18. Eta Model output heights (m), temperatures (°C), and winds (as in Fig. 2) at 500 hPa at (a) 1200 and (b) 0000 UTC.

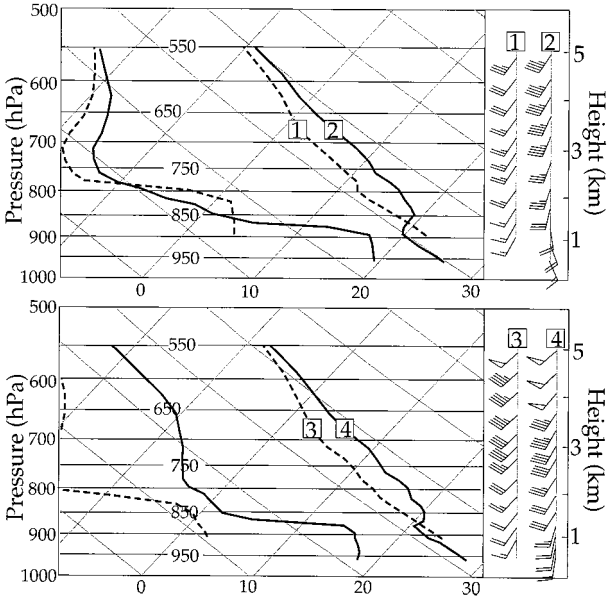


FIG. 19. Eta Model soundings at 1800 UTC at the locations noted in Fig. 20b. Temperature and dewpoint temperature are shown. Winds are plotted as in Fig. 6.

scale that may be used to determine the location and motion of a narrow region within which the dryline exists.

In Fig. 18 the Eta Model initial and 12-h forecast 500-hPa height, temperature, and winds are plotted, valid at 1200 UTC on 16 May and 0000 UTC on 17 May, respectively. These fields can be compared with the observed analyses shown in Fig. 3. The model initial fields appear to agree quite well with the analysis; the location of the low center in southeast Colorado can be determined with greater accuracy in the model case owing to the greater density of data points. The 12-h forecast fields appear to agree quite well also. The motion of the low center and trough, as well as the filling of the low, are predicted accurately. Forecast winds are generally within 2.5 m $s^{-1}$ of the observed wind magnitudes and agree in direction quite well for all but the very low speed range.

It is more difficult to compare the vertical profiles between model and observed fields. To provide an example of model across-dryline variations in vertical profiles, four soundings are plotted in Fig. 19. These are all model forecast soundings at 1800 UTC whose locations are shown later (Fig. 21b). Because of the 32-km grid spacing in the model, the sharp gradients along the dryline (in nature) are not resolved by the model. The across-dryline distance between the two pairs of model soundings shown is about 225 km (seven grid distances). Few significant differences can be seen between the northern and the southern sounding pairs (i.e., comparing 1 with 3 and 2 with 4). Winds from the southern pair (3 and 4) are slightly stronger because the northern pair is nearer to the upper low center. Across-dryline variations are typical of those in the dryline near-environment. In the moist air there is a moist mixed layer 60–80 hPa in depth near the surface topped by a stable layer above which rapid drying occurs. Winds veer with height slowly through the moist layer, then rapidly through the stable layer above. In the dry air there is a deep adiabat layer near the surface with nearly unidirectional winds throughout and only modest speed increases with height, all characteristic of an air mass that has undergone strong vertical mixing in the near-surface boundary layer.

A direct comparison of a model sounding and an observed sounding in the dry air is shown in Fig. 20. Few observed soundings were taken in the moist air, and those that were obtained were judged not representative of moist side conditions for one reason or another.

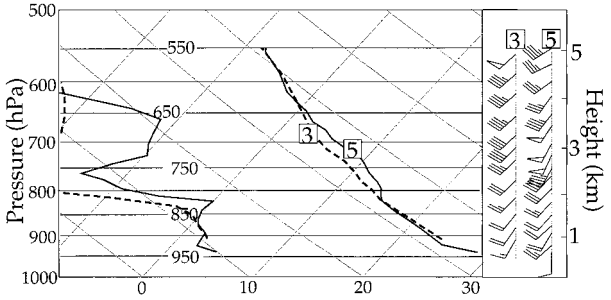


FIG. 20. As in Fig. 19 but observed (solid) and model (dashed) soundings at 1800 UTC at the locations noted in Fig. 21b.

The locations of the two soundings is indicated in Fig. 21b. The agreement in temperature, moisture, and winds is quite close in low levels below 820 hPa. The observed sounding includes a stable layer based at about 820 hPa that is much less pronounced in the model sounding. Temperatures are therefore 1°–1.5°C warmer in the observed sounding from about 800 to 650 hPa. The observed sounding is slightly more moist in this layer and winds are slightly stronger and more backed.

Moving from the upper air to the surface, an example of the model output surface moisture field is shown in Fig. 21a. As noted previously the dryline is depicted as a broad zone of enhanced moisture gradient owing to the limited model resolution. The field shown is the specific humidity (g kg$^{-1}$) diagnostically derived at 10 m above ground level (AGL) from model output at 2200 UTC in a manner consistent with the surface layer physical parameterization. This diagnostic calculation used the model boundary layer turbulent parameterization to determine vertical profiles of wind, temperature, and moisture consistent with surface fluxes, stability, etc. Also shown are surface (10 m AGL) wind vectors at reduced resolution indicating the general horizontal flow. The motion of the modeled dryline is shown in Fig. 21b through an isochrone analysis at 2-h intervals from 1200 to 0000 UTC. Also indicated in the figure are the observed dryline positions at 1800, 2000, and 2200 UTC. For simplicity, the 13 g kg$^{-1}$ contour of specific humidity output by the model was used to identify the dryline. This contour was located near the eastern edge of the enhanced moisture gradient at all forecast output times.

The modeled dryline's rapid eastward displacement (Fig. 21b) between 1200 and 1400 UTC differed greatly from the observed motion and is discussed below. By 1800 UTC the model dryline's location over Oklahoma was in reasonably good agreement with observations (Fig. 21b). After 1600 UTC motion of the model dryline toward the east was more regular. Based upon surface, radar, and aircraft observations, the dryline ''jumped'' eastward in central Oklahoma between 1900 and 2000 UTC owing to a combination of continuous motion and redevelopment. There was also a large displacement in the same region in the model results between 1800 and

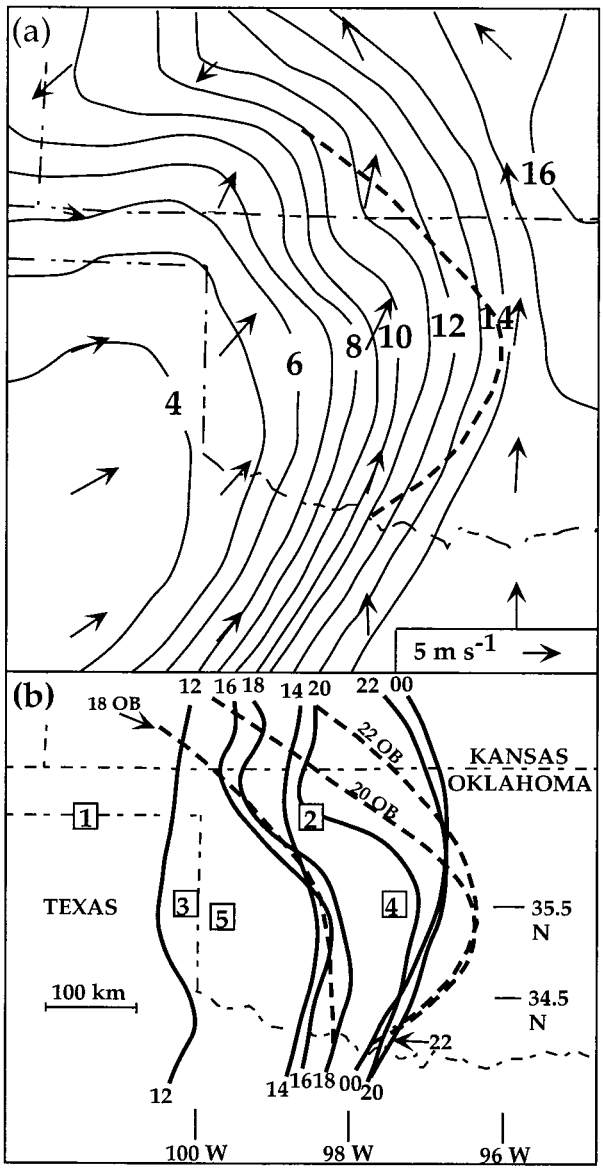


FIG. 21. (a) Specific humidity (g kg$^{-1}$) at surface from Eta Model at 2200 UTC. Scale of horizontal wind vectors is indicated at lower right. The dashed curve indicates the observed dryline location at this time. (b) Dryline isochrones at two hour intervals from Eta Model simulation (solid). Also shown are observed dryline locations at 1800, 2000, and 2200 UTC (dashed). Boxed numbers indicate locations of soundings in Figs. 19 and 20.

2000 UTC, but not as large as that observed. In northern Oklahoma and southern Kansas between 2000 and 2200 UTC the model dryline moved eastward much more rapidly than observed. Late in the afternoon there was slow westward motion (retreat) of the dryline in the southern part of the domain, as there was in the observed fields. However, the jump to the west between 2300 and 0000 UTC in the observations was absent in the model results.

The modeled motion of the dryline (based upon 10

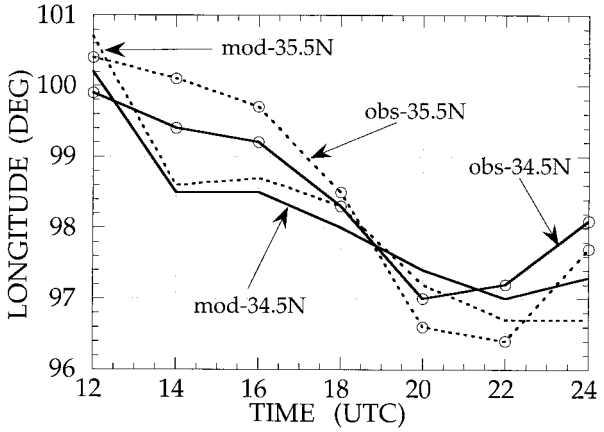


FIG. 22. Longitude of modeled and observed drylines as a function of time. Solid curves are at 34.5°N and dashed at 35.5°N. Curves marked with circles are observed.

m AGL fields) is summarized in a different way in Fig. 22. Here the longitude of dryline location is plotted at two latitudes corresponding to central and southern Oklahoma (these latitudes are indicated in Fig. 21b). The observed dryline motion is also included for comparison. The rapid motion of the dryline toward the east (downward trend of curves) that occurred between 1200 and 1400 UTC in the model case resulted from vertical mixing of a thin layer of moisture near the surface. The difference from observations in this period is an indication that the layer of moisture near the surface was initialized over a depth that was too small or that the model does not accurately account for mixing of thin surface moist layers. Both the model and observations show rapid dryline motion toward the east in the 1600–2000 UTC period, likely a result of efficient vertical mixing during midday (to be explored in more detail below). In central and southern Oklahoma dryline motion and location during the 1600–2200 UTC period were simulated quite accurately, but discrepancies were present in extreme northern Oklahoma and southern Kansas, as noted above.

### *c. Model moisture convergence and vertical motion*

The modeled evolutions of the moisture convergence and vertical motion fields in the dryline region were also examined. Moisture convergence was computed using mass-weighted average winds and specific humidity from model layers in the lowest 30 mb above the model topography. In the early morning an axis of moisture convergence extended southeastward through central Oklahoma from a maximum in northwest Oklahoma ahead of the dryline (not shown). The maximum weakened during late morning, and only the axis through central Oklahoma remained at midday. By 2000 UTC there was a prominent convergent axis that coincided fairly well with the model dryline location following its rapid eastward motion. This convergent axis persisted through the afternoon and moved steadily eastward generally with the dryline in the northern domain, and was nearly stationary in the south.

Locations of model moisture convergence axes and the model dryline in the area of primary interest, in addition to the vertical motion field at 800 hPa, are shown in Fig. 23 at two times. At 1800 UTC there was a moisture convergence axis through central Oklahoma as described above. A second axis to the north that appears to have been rotating around the synoptic low is also indicated. The convergence axis in central Oklahoma was well to the east of the model dryline at 1800 UTC. There was some indication in the observed fields also that a convergent axis may have been present in this same area; however, observational sites were too widely spaced to ascertain its strength or exact location. The installation of the Oklahoma Mesonetwork (Brock et al. 1995) occurred following the COPS-91 field program; therefore, the analysis of cases similar to this one could now be carried out using that dataset to explore this issue.

At 2200 UTC (Fig. 23b) the model dryline and convergence axis were more nearly collocated. With regard to the aircraft observations discussed in the last section, the possibility exists that preexisting convergence may have been the factor that dictated where the series of ''moisture steps'' terminated on the east (at the reestablished dryline location). This line of reasoning is also compatible with previous work (Crawford and Bluestein 1997) where it has been shown that the dryline generally is located on the west edge of a pressure trough in the morning, and later in the day advances through the trough (e.g., see Fig. 2).

The model output vertical motion field was also examined in relation to dryline motion. It has been hypothesized in the case of dryline bulges (Tegtmeier 1974) that in some cases the synoptic- or subsynoptic-scale downward motion associated with a translating upper-level disturbance may enhance the downward flux of horizontal momentum west of the dryline and thereby enhance horizontal advection (Schaefer 1986). The model vertical motion field was examined at a number of levels of constant pressure and in vertical cross sections. The 800-hPa level was considered representative of larger-scale conditions just above the boundary layer, at least from central Oklahoma eastward. At all times there was a maximum of downward motion in northwest Texas, as shown for example in both panels of Fig. 23. Taking into account both the strength and direction of the boundary layer winds, this maximum is interpreted as flow down the relatively higher terrain in this area. At 1800 UTC and earlier this area was near the dryline and could have been influential in the formation of the bulge. However, to the extent that the model output is accurate, it appears that in this case for the remainder of the day downward motion just west of the dryline cannot be implicated in the rapid dryline motion and displacement. As is exemplified in Fig. 23b, and at all

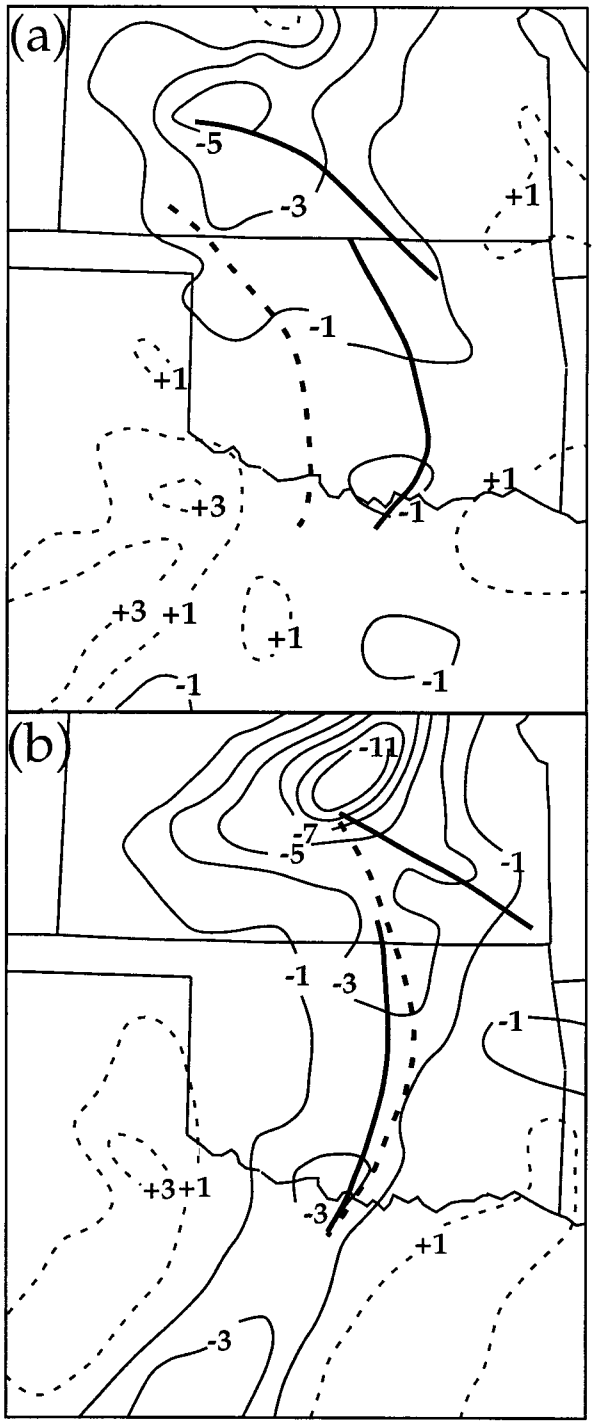


FIG. 23. Eta Model output 800-hPa omega field (Pa $s^{-1}$) at (a) 1800 and (b) 2200 UTC. Model dryline locations are indicated by heavy dashed line. Model moisture convergence axes are denoted by heavy solid lines. Model upward motion is contoured with solid lines and downward motion with dashed.

times following 1800 UTC, the area of downward motion was far to the west of the dryline. This separation is not merely a matter of lack of model resolution; the couplet in north-central Kansas in Fig. 23a, for example, demonstrates the model's ability to resolve small-scale features.

In Fig. 23a there are two axes of upward motion extending from the center associated with the upper short-wave trough. One extends southward from the center through southwest Kansas into northwest Oklahoma, and the other from the center across south-central Kansas into east-central Oklahoma. By 2200 UTC (Fig. 23b) these axes had progressed with the moving center to locations nearly coincident with the two convergence axes. It appears that the southern extension of the northwest Oklahoma vertical velocity axis at 1800 UTC is masked by the downslope flow over northwest Texas. By 2200 UTC this axis has moved into central Oklahoma east of the area of downslope flow. The axis of surface convergence ahead of the dryline at 1800 UTC appears to have redeveloped westward by 2200 UTC in response to the upward motion axis. By this time the dryline circulation itself likely had strengthened and may have been contributing to the increased organization of the vertical motion axis in Fig. 23b.

### *d. Physical processes influencing model dryline motion*

The Eta Model simulated with reasonable accuracy dryline motion and location in central and southern Oklahoma during the afternoon on this day. Therefore, in order to provide additional insight into the physical processes that were governing dryline motion, diagnosis of model output was undertaken. The formula for the motion of an isobar given by Bluestein (1992, p. 51) is valid for any scalar. If it is assumed that the dryline is identified with a given isopleth of specific humidity, and dryline motion is nearly constant for short periods (on the order of 10 min), then it may be shown that the motion of the dryline can be expressed

$$c = -\frac{S}{\left(\frac{\partial q}{\partial x}\right)}, \tag{1}$$

where $c$ is dryline motion (positive toward the east), $q$ is specific humidity, and $S$ represents the sum of all terms contributing to local time changes in the continuity equation for specific humidity. Specifically, $S$ includes from the Eta Model equation, horizontal and vertical advection (Black et al. 1997; Mesinger and Janjić 1990), vertical mixing and surface exchanges (Chen et al. 1996; Janjić 1996a,b), horizontal mixing (Janjić 1990), and effects of parameterized shallow convective clouds (Betts and Miller 1986; Janjić 1994; Zhao et al. 1997).

The longitudes of two specific humidity contours at

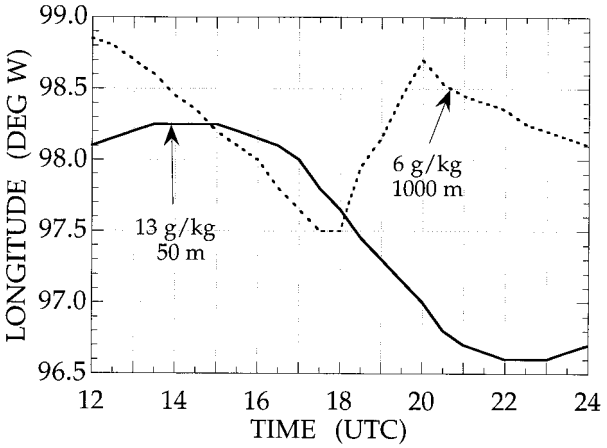


FIG. 24. Longitude of model specific humidity contours as a function of time of day at 35.5°N. The 13 g kg$^{-1}$ contour at 50 m AGL (solid) and 6 g kg$^{-1}$ contour at 1000 m AGL are shown.

35.5°N as a function of time of day are shown in Fig. 24. The 13 g kg$^{-1}$ contour at 50 m AGL was chosen to represent the location of the dryline in the lower boundary layer, and the 6 g kg$^{-1}$ contour at 1000 m AGL to gauge the motion of dry air that was initially above the moist layer east of the dryline. If the 13 g kg$^{-1}$ curve in Fig. 24 is compared to that in Fig. 22 (mod-35.5N), it is clear that the location of this contour at 50 m AGL is much farther east than that at 10 m AGL (an indication of the extreme shallowness of the model moist layer early in the day). After retreating a short distance to the west the 13 g kg$^{-1}$ contour (dryline at 50 m AGL) advanced eastward during the late morning and afternoon with most rapid motion between 1700 and 2100 UTC. The dry air at 1000 m AGL (dashed curve in Fig. 24) overtook and moved east of the dryline in the 1200–1700 UTC period. At about 1800 UTC the boundary layer mixed above the 1000 m AGL level and effectively pushed the 6 g kg$^{-1}$ contour back to the west. As boundary layer growth ceased, the dry air began to move steadily to the east at this level after 2000 UTC.

The contributions of individual physical processes to the motion of the model 13 and 6 g kg$^{-1}$ specific humidity contours at different times, based upon calculation of (1), are shown in Fig. 25. Gridded model output was interpolated in space and time to the needed locations and common time resolution for individual terms, then averaged over 6-min intervals. The motion of the 13 g kg$^{-1}$ contour at $z = 50$ m is shown to have been dominated by vertical turbulent mixing and surface exchanges (VT in Fig. 25a) during the period of rapid eastward dryline motion (1700–2030 UTC). Horizontal advection and horizontal diffusion had roughly equal and opposite effects at this level until about 1900 UTC. Vertical advection of specific humidity was generally weak, though a small amount of positive contribution to eastward motion was realized owing to a thin localized layer of subsidence near the surface after 2000

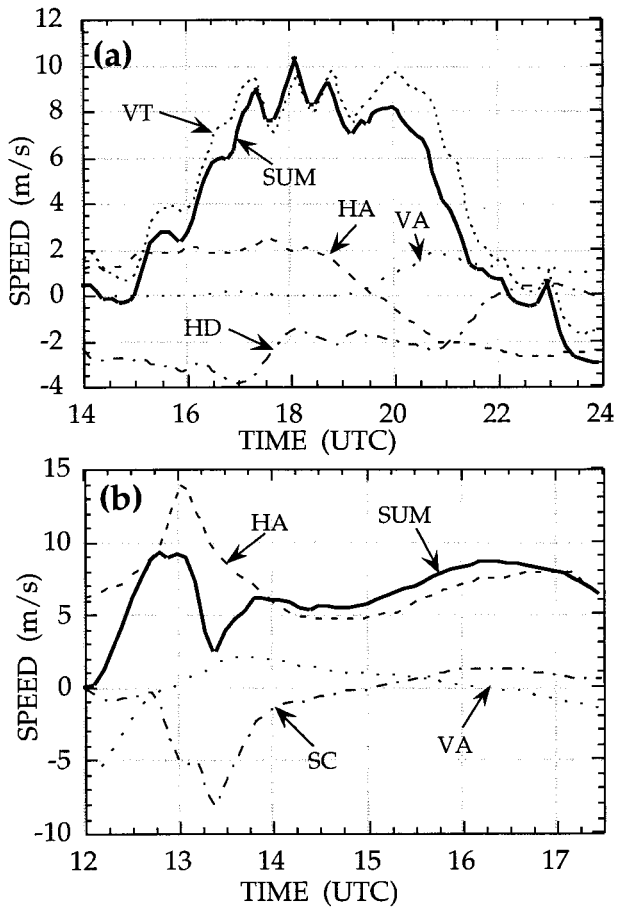


FIG. 25. Contributions to the speed (SUM) of model specific humidity contours at 35.5°N including (a) 13 g kg$^{-1}$ at $z = 50$ m AGL and (b) 6 g kg$^{-1}$ at $z = 1000$ m AGL. Contributing physical processes include HA, horizontal advection; VA, vertical advection; VT, vertical turbulent mixing including surface exchanges; HD, horizontal diffusion; and SC, parameterized shallow cumulus convection.

UTC. This thin layer was not linked to larger-scale subsidence at 800 hPa discussed in section 5c. Horizontal advection of dry air ceased at about 1930 UTC and moist advection continued through 0000 UTC, eventually resulting in westward dryline motion after 2300 UTC following the rapid decline in vertical mixing. Comparing the late afternoon retreat of the model dryline to observations, it is clear that the westward redevelopment was not captured. The model cannot account for small-scale processes that were occurring in nature; however, it did capture the slow, continuous westward motion of the dryline at this latitude, and included a strong influence of the diurnal heating cycle among the contributions to that motion.

The contributions to eastward motion of the 6 g kg$^{-1}$ contour at 1000 m AGL are shown in Fig. 25b during the morning period before boundary layer mixing encompassed this level. Motion was clearly dominated by horizontal advection of dry air from the west during this period. Both vertical turbulent mixing and horizontal

diffusion were very small (not plotted), and vertical advection was also small. Shallow convection significantly slowed eastward motion in the 1300–1400 UTC period. This level was near the top of a parameterized layer of shallow convection, resulting in locally increased specific humidity. Later in the morning this shallow layer ascended, so that the 1000-m level was near the layer base, and a small drying tendency was realized.

In summary, the assessment of contributions by various physical processes toward model dryline motion revealed that vertical mixing was the major factor in advancing the dryline rapidly eastward during the middle of the day. However, the role of horizontal advection of dry air *aloft* was vital in this synoptically influenced case. Advection of dry air aloft above and just to the east of the dryline location was a *major* reason for the effectiveness of vertical mixing in advancing the dryline rapidly eastward. Whether these model results aid in understanding the contributions to motion of the observed dryline on this day depends on many factors including the degree of realism with which vertical turbulent mixing and other physical processes are accounted for in the Eta Model. The reasonably accurate simulation of dryline location, the strong signal in the model results, and physical plausibility are all factors favoring acceptance of the above explanation.

## 6. Summary and discussion

### *a. Major findings*

Through a case study approach, issues have been examined that are related to the motion of and multiple moisture gradients near a dryline that occurred in a synoptically active environment on 16 May 1991. Basic insights into multiple moisture gradients in the dryline environment and ''jumps'' in dryline location are of great interest to operational meteorologists who must not only analyze current observational fields that contain such features, but also nowcast their behavior and any convection that develops in association with them. In addition, the output of an operational mesoscale model was compared with observations, not only to check the ability of the model to forecast dryline features, but to help interpret the observational analysis.

The dryline moved rapidly across the western two-thirds of Oklahoma on this day and was well tracked by surface network, profiler, research aircraft, research sounding, radar, and satellite data. A subsynoptic-scale dryline bulge to the east-northeast began to develop at about 1800 UTC in central Oklahoma. Redevelopment of the dryline at a new location to the east occurred along a portion of the bulge between 1900 and 2000 UTC. A vertical cross section derived from an aircraft traverse pattern verified the location of the dryline just prior to the eastward jump. A series of steps representing increasing moisture depth toward the east was then identified by the aircraft, the last step being the relocated dryline signature. Radar observations indicate that the steps coincide with thinlines that extend over distances of 100 km or more approximately parallel to the dryline. The step representing the earlier dryline location also continued moving steadily toward the east. The steps possibly result from circulations about axes that are quasi-parallel to the dryline, perhaps excited by the original dryline's disturbance of the flow or perhaps indicating the superposition of convective boundary layer rolls; more detailed measurements are needed for additional insight.

The retreat of the dryline in late afternoon and evening in central Oklahoma was diagnosed by radar clear air data and included continuous motion toward the west-northwest of two major boundaries and a westward redevelopment of the dryline. Additionally, radar revealed the presence of other thinlines that were approximately parallel to the major boundaries and moved with them. An analysis based upon an aircraft vertically stepped pattern along the northern edge of the region of redevelopment and through the easternmost thinline verified the existence of the dryline at that location. There were additional gradients associated with a thinline about 13 km to the west within the cross section. To the authors, knowledge this is the first observation of multiple thinlines in the dryline environment through the depth of the boundary layer by both aircraft and radar.

Based upon clear air Doppler radial velocity measurements, the evolution of the wind field was gradual in the 80-km-wide region between the late-afternoon location of the dryline (where storms developed) and the location to the west where the dryline redeveloped. Winds backed from south-southwesterly to south-southeasterly in the lower 2 km of the atmosphere. Soundings taken within the same region showed a backing and strengthening of low-level winds and a low-level increase in moisture. A part of this change was likely linked to the diurnal cycle in the evening dryline environment. The resulting moist layer was shallower, however, than that in the early afternoon east of the dryline. Moreover, warming and drying took place above the moist layer as a result of either subsidence or horizontal advection from the west.

An Eta Model run initialized at 1200 UTC produced a forecast of dryline features that was reasonably accurate over central and southern Oklahoma. The motion and evolution of midtropospheric fields were well forecast, and the eastward motion of a broad (owing to model resolution) region of enhanced east–west moisture gradient agreed reasonably well with observations in late morning and afternoon. Determination of whether this model consistently forecasts the dryline environment well would require a separate study of many cases. An identifiable north–south moisture convergence axis preceded the rapid eastward motion of the dryline (which in the observations involved loss in definition at one location and gain at another, as noted above) by

several hours. Model vertical motion fields indicated subsidence west of the dryline in the early morning, which gave way to ascending motion by midday. Therefore the role of subsidence west of the dryline in this case in influencing rapid eastward motion (e.g., the bulge) appears absent in this case, and the roles of horizontal advection and turbulent vertical mixing paramount. The model results *do* show the importance of vertical mixing and surface processes in contributing to dryline motion and evolution. Calculation of modeled physical mechanisms produced a clear indication that both vertical mixing in the boundary layer and horizontal advection of dry air aloft in this synoptically active case are essential ingredients in rapid dryline motion.

### *b. Discussion*

This work, while investigating dryline motion in an active synoptic environment through a unique set of observations and bringing to light a number of new findings, leaves other questions unanswered. Any description of the overall picture must therefore contain some degree of uncertainty. The two major factors controlling dryline motion in this case were vertical mixing in the dry air and enhanced upper-level flow associated with a short-wave trough. The vertical mixing is tied strongly to the diurnal cycle while the short wave, at least directly, is not. It may be, therefore, that the evolution and motion of the dryline would be somewhat different if a short-wave trough were to reach the area at other times of day.

In this case, as the synoptic disturbance passed over the edge of the moist air (dryline) from west to east, it apparently enhanced convergence in the lee pressure trough (becoming most evident at about 1800 UTC) within the moist air to the east of the dryline (defined by the moisture gradient) at the same time that strong synoptically forced winds and vertical mixing farther west were advancing the moisture gradient eastward. With intense heating near midday and continued strong winds the moisture gradient advanced rapidly eastward and by 2000 UTC or so caught up with the convergent region. The final step in this ''catch-up'' process was redevelopment, where the convergence near the dryline decreased, but did not entirely disappear, and the preexisting convergence zone (present in model output and likely in nature) effectively became the new dryline location approximately 120 km to the east. Also evident were ''steps'' in the depth of the moisture between the two features that may have been excited by the original dryline circulation (this remains to be determined by future research). The redevelopment process has been documented in other dryline cases, though the distances over which it occurs varies from one case to another. A potential topic for future research concerns how differing environments influence the redevelopment process.

In late afternoon at the dryline's most eastward location thunderstorms were initiated. As illustrated in Fig. 4, the dryline to the north of this thunderstorm area continued its northeastward motion in association with the synoptic system in Kansas, while the dryline to the south retreated slightly toward the west-northwest between 2000 and 2300 UTC. Between 2300 and 0000 UTC the southern portion of the dryline jumped westward as indicated in Fig. 4 to approximately its 1900 UTC location. It appears likely that the waning influence of the synoptic disturbance on the wind field (as it moved to the northeast and westerly wind component west of the dryline decreased) and the cessation of strong vertical mixing in the dry air combined to produce a loss of dryline characteristics at the eastern location and redevelopment to the west.

The observation of the above-mentioned westward redevelopment process brings about another question: Through what mechanism was this moisture gradient (accompanied by some convergence) maintained through 4 h or so at the more western location? The answer to this and other issues, such as those relating to the cause of stepped features in the moist air and details of how the observed jumps take place, will have to await (a) field efforts that include added temporal and spatial resolution and (b) associated carefully planned mesoscale modeling efforts.

*Acknowledgments.* The authors thank D. Burgess and J. LaDue for providing access to recorded KTLX radar data. Comments on an earlier version of the manuscript were provided by J. Kain, D. Burgess, and J. Hales, contributing to numerous improvements. Two anonymous, thoughtful reviews provided suggestions that resulted in substantial improvements in the manuscript. The accomplishment of field experiments was made possible by scientific crews on the P-3 aircraft and in M-CLASS vehicles, including the following individuals: D. Bartels, H. Bluestein, M. Douglas, S. Fredrickson, C. George, C. Hane, D. Jorgensen, S. Koch, W. Martin, J. Meitin, T. Shepherd, L. Showell, T. Shuur, B. Smull, M. Stolzenburg, G. Stumpf, A. Watson, Q. Xu, and C. Ziegler. We are grateful to the flight crew of NOAA's Office of Aircraft Operations for their support. M. Shapiro and M. Douglas provided valuable suggestions in the planning of aircraft patterns. Thanks are given to J. O'Bannon for aiding in the preparation of figures. The PAM network was provided by the Atmospheric Technology Division of NCAR, which is sponsored by the National Science Foundation (NSF). The PAM network received partial support from the National Aeronautics and Space Administration through the efforts of S. Koch. A portion of the work was supported by Grants ATM-9019821, ATM-9302379, and ATM-9612674 to the University of Oklahoma from the NSF.

## REFERENCES


Atkins, N. T., R. M. Wakimoto, and C. L. Ziegler, 1998: Observations of the finescale structure of a dryline during VORTEX 95. *Mon. Wea. Rev.,* **126,** 525–550.

Betts, A. K., and M. J. Miller, 1986: A new convective adjustment scheme. Part II: Single column tests using GATE wave, BOMEX, ATEX, and arctic air-mass data sets. *Quart. J. Roy. Meteor. Soc.,* **112,** 693–709.

——, F. Chen, K. E. Mitchell, and Z. I. Janjić, 1997: Assessment of the land surface and boundary layer models in two operational versions of the NCEP Eta Model using FIFE data. *Mon. Wea. Rev.,* **125,** 2896–2916.

Black, T. L., 1994: The new NMC mesoscale Eta Model: Description and forecast examples. *Wea. Forecasting,* **9,** 265–278.

——, and Coauthors, 1997: Changes to the Eta forecast systems. NWS Tech. Procedures Bull. 441, NOAA/NWS, 31 pp. [Available from Office of Meteorology, National Weather Service, 1325 East–West Highway, Silver Spring, MD 20910.]

Bluestein, H. B., 1992: *Synoptic Dynamic Meteorology in Midlatitudes,* Vol. 1, *Principles of Kinematics and Dynamics.* Oxford University Press, 421 pp.

——, and T. M. Crawford, 1997: Mesoscale dynamics of the near-dryline environment: Analysis of data from COPS-91. *Mon. Wea. Rev.,* **125,** 2161–2175.

——, E. W. McCaul Jr., G. P. Byrd, and G. R. Woodall, 1988: Mobile sounding observations of a tornadic storm near the dryline: The Canadian, Texas storm of 7 May 1986. *Mon. Wea. Rev.,* **116,** 1790–1804.

——, ——, ——, ——, G. Martin, S. Keighton, and L. C. Showell, 1989: Mobile sounding observations of a thunderstorm near the dryline: The Gruver, Texas storm complex of 25 May 1987. *Mon. Wea. Rev.,* **117,** 244–250.

Brock, F. V., G. Saum, and S. Semmer, 1986: Portable Automated Mesonet II. *J. Atmos. Oceanic Technol.,* **3,** 573–582.

——, K. C. Crawford, R. L. Elliott, G. W. Cuperus, S. J. Stadler, H. L. Johnson, and M. D. Eilts, 1995: The Oklahoma Mesonet: A technical overview. *J. Atmos. Oceanic Technol.,* **12,** 5–19.

Chadwick, R., 1988: The wind profiler demonstration network. *Extended Abstracts, Symp. on Lower Tropospheric Profiling: Needs and Technologies,* Boulder, CO, Amer. Meteor. Soc., 109–110.

Charney, J. J., and J. M. Fritsch, 1999: Discrete frontal propagation in a nonconvective environment. *Mon. Wea. Rev.,* **127,** 2083–2101.

Chen, F., and Coauthors, 1996: Modeling of land-surface evaporation by four schemes and comparison with FIFE results. *J. Geophys. Res.,* **101,** 7251–7268.

Crawford, T. M., and H. B. Bluestein, 1997: Characteristics of dryline passage during COPS-91. *Mon. Wea. Rev.,* **125,** 463–477.

Fujita, T. T., 1970: The Lubbock tornadoes: A study of suction spots. *Weatherwise,* **23,** 160–173.

Grossman, R. L., 1982: An analysis of vertical velocity spectra obtained in the BOMEX fair-weather, trade-wind boundary layer. *Bound.-Layer Meteor.,* **23,** 323–357.

Hane, C. E., C. L. Ziegler, and H. B. Bluestein, 1993: Investigation of the dryline and convective storms initiated along the dryline: Field experiments during COPS-91. *Bull. Amer. Meteor. Soc.,* **74,** 2133–2145.

——, H. B. Bluestein, T. M. Crawford, M. E. Baldwin, and R. M. Rabin, 1997: Severe thunderstorm development in relation to along-dryline variability: A case study. *Mon. Wea. Rev.,* **125,** 231–251.

Janjić, Z., 1990: The step-mountain coordinate: Physical package. *Mon. Wea. Rev.,* **118,** 1429–1443.

——, 1994: The step-mountain eta coordinate model: Further developments of the convection, viscous sublayer, and turbulence closure schemes. *Mon. Wea. Rev.,* **122,** 927–945.

——, 1996a: The surface parameterization in the NCEP Eta model. Research Activities in Atmospheric and Oceanic Modeling. CAS/JSC Working Group on Numerical Experimentation, WMO, 440 pp. [Available from WMO, CP No. 2300, CH-1211, Geneva 2, Switzerland.]

——, 1996b: The Mellor–Yamada level 2.5 turbulence closure scheme in the NCEP Eta Model. Preprints, *11th Conf. on Numerical Weather Prediction,* Norfolk, VA, Amer. Meteor. Soc., 333–334.

Kalnay, E., and Coauthors, 1996: The NCEP/NCAR 40-Year Reanalysis Project. *Bull. Amer. Meteor. Soc.,* **77,** 437–471.

LeMone, M. A., 1973: The structure and dynamics of horizontal roll vortices in the planetary boundary layer. *J. Atmos. Sci.,* **30,** 1077–1091.

Marks, F., Jr., and R. Houze, Jr., 1987: Inner core structure of Hurricane Alicia from airborne Doppler radar observations. *J. Atmos. Sci.,* **44,** 1296–1317.

McGinley, J. A., and Y. K. Sasaki, 1975: The role of symmetric instabilities in thunderstorm development on drylines. Preprints, *Ninth Conf. on Severe Local Storms,* Norman, OK, Amer. Meteor. Soc., 173–180.

Mesinger, F., and Z. I. Janjić, 1990: Numerical methods used in atmospheric models. GARP Publ. Series, Vol. 1, No. 17, WMO, 64 pp. [Available from WMO/ICSU, Case Postale No. 2300, CH-1121 Geneva 20, Switzerland.]

Parsons, D. B., M. A. Shapiro, R. M. Hardesty, R. J. Zamora, and J. M. Intrieri, 1991: The finescale structure of a west Texas dryline. *Mon. Wea. Rev.,* **119,** 1242–1258.

Rogers, E., and Coauthors, 1997: Changes to the NCEP Operational ''Early'' Eta Analysis/Forecast System. NWS Tech. Procedures Bull. 447, National Oceanic and Atmospheric Administration/National Weather Service, 14 pp. [Available from Office of Meteorology, National Weather Service, 1325 East–West Highway, Silver Spring, MD 20910.]

Rust, W. D., D. W. Burgess, R. A. Maddox, L. Showell, T. Marshall, and D. Lauritzen, 1990: Testing a mobile version of a Cross-Chain LORAN Atmospheric (M-CLASS) Sounding System. *Bull. Amer. Meteor. Soc.,* **71,** 173–180.

Schaefer, J. T., 1974a: The life cycle of the dryline. *J. Appl. Meteor.,* **13,** 444–449.

——, 1974b: A simulative model of dryline motion. *J. Atmos. Sci.,* **31,** 956–964.

——, 1986: The dryline. *Mesoscale Meteorology and Forecasting,* P. S. Ray, Ed., Amer. Meteor. Soc., 549–572.

Shaw, B. L., R. A. Pielke, and C. L. Ziegler, 1997: A three-dimensional numerical simulation of a Great Plains dryline. *Mon. Wea. Rev.,* **125,** 1489–1506.

Tegtmeier, S. A., 1974: The role of the surface, sub-synoptic, low pressure system in severe weather forecasting. M. S. thesis, School of Meteorology, University of Oklahoma, Norman, OK, 66 pp.

Weckwerth, T. M., J. W. Wilson, R. M. Wakimoto, and N. A. Crook, 1997: Horizontal convective rolls: Determining the environmental conditions supporting their existence and characteristics. *Mon. Wea. Rev.,* **125,** 505–526.

——, T. W. Horst, and J. W. Wilson, 1999: An observational study of the evolution of horizontal convective rolls. *Mon. Wea. Rev.,* **127,** 2160–2179.

Zhao, Q., T. L. Black, and M. E. Baldwin, 1997: Implementation of the cloud prediction scheme in the Eta Model at NCEP. *Wea. Forecasting,* **12,** 697–712.

Ziegler, C. L., and C. E. Hane, 1993: An observational study of the dryline. *Mon. Wea. Rev.,* **121,** 1134–1151.

——, W. J. Martin, R. A. Pielke, and R. L. Walko, 1995: A modeling study of the dryline. *J. Atmos. Sci.,* **52,** 263–285.

——, T. J. Lee, and R. A. Pielke Sr., 1997: Convective initiation at the dryline: A modeling study. *Mon. Wea. Rev.,* **125,** 1001–1026.